SANDIA REPORT
SAND2019-XXXX
Unlimited Release
Printed Month and Year

Material Property Determinations for Alluvium in Support of Source Physics Experiment

Scott T. Broome, Perry C. Barrow, Johnny L. Jaramillo

Prepared by
Sandia National Laboratories
Albuquerque, New Mexico 87185 and Livermore, California 94550

Sandia National Laboratories is a multimission laboratory managed and operated by National Technology and Engineering Solutions of Sandia, LLC, a wholly owned subsidiary of Honeywell International, Inc., for the U.S. Department of Energy's National Nuclear Security Administration under contract DE-NA0003525.

Issued by Sandia National Laboratories, operated for the United States Department of Energy by National Technology and Engineering Solutions of Sandia, LLC.

Available to DOE and DOE contractors from

U.S. Department of Energy
Office of Scientific and Technical Information
P.O. Box 62
Oak Ridge, TN 37831

Telephone: (865) 576-8401
Facsimile: (865) 576-5728
E-Mail: reports@osti.gov
Online ordering: http://www.osti.gov/scitech

Available to the public from

U.S. Department of Commerce
National Technical Information Service
5301 Shawnee Rd
Alexandria, VA 22312

Telephone: (800) 553-6847
Facsimile: (703) 605-6900
E-Mail: orders@ntis.gov
Online order: https://classic.ntis.gov/help/order-methods/

This page is intentionally left blank.

SAND2019-10645
Printed September 2019
Unlimited Release

Material Property Determinations for Alluvium in Support of Source Physics Experiment

Scott T. Broome, Perry C. Barrow, Johnny L. Jaramillo
Geomechanics (08864)
Sandia National Laboratories
PO Box 5800, MS 1033
Albuquerque, New Mexico 87185-1033

ABSTRACT

Two blocks of alluvium were extensively tested at the Sandia National Laboratories Geomechanics laboratory. The alluvium blocks are intended to serve as surrogate material for mechanical property determinations to support the SPE DAG experimental series. From constant mean stress triaxial testing, strength failure envelopes were parameterized and are presented for each block. Modulus and stress relationships are given including bulk modulus versus mean stress, shear modulus versus shear stress, Young's modulus versus axial stress and Poisson's ratio versus axial stress. In addition, P-&S-wave velocities, and porosity, determined using helium porosimetry, were obtained on each block.

Generally, both Young's modulus and Poisson's ratio increase with increasing axial stress, bulk modulus increases with increasing pressure, and increases more dramatically upon pore crush, shear modulus decreases with increasing shear stress and then appears to plateau. The Unconfined Compressive Strength for the BM is in the range of 0.5-0.6, and for SM in the range of 2.0-2.6 MPa. The confined compressive strength increases with increasing confining pressure, and the BM alluvium is significantly weaker compared to SM alluvium for mean stress levels above 8 MPa.

ACKNOWLEDGEMENTS

The authors would like to thank Steve Bauer and Moo Lee for their critical reviews of the report.

The authors acknowledge the support of the National Nuclear Security Administration Office of Defense Nuclear Nonproliferation Research and Development for funding this work. This paper describes objective technical results and analysis. Any subjective views or opinions that might be expressed in the paper do not necessarily represent the views of the U.S. Department of Energy or the United States Government.

TABLE OF CONTENTS

FIGURES

TABLES

NOMENCLATURE

Abbreviation	Definition
DAG	Dry Alluvium Geology
SPE	Source Physics Experiment
NNSS	Nevada National Security Site
SNL	Sandia National Laboratories
SM	Alluvium block 092817-U1a.104-A
BM	Alluvium block 092817-U1a.104-B
CMS	Constant Mean Stress triaxial test
UCS	Unconfined Compressive Strength

1. INTRODUCTION

The Nevada National Security Site (NNSS) serves as the geologic setting for a Source Physics Experiment (SPE) program. The SPE provides ground truth data to create and improve strong ground motion and seismic S-wave generation and propagation models. The NNSS was chosen as the test bed because it provides a variety of geologic settings ranging from relatively simple to very complex.

Each series of SPE testing will comprise the setting and firing of explosive charges (source) placed in a central borehole at varying depths and recording ground motions in instrumented boreholes located in two rings around the source, positioned at different radii. Modeling using advanced simulation codes will be performed both before and after each test to predict ground response and to improve models based on acquired field data, respectively.

A key component in the predictive capability and ultimate validation of the models is the full understanding of the intervening geology between the source and the instrumented boreholes including the geomechanical behavior of the site's rock/structural features. This document reports on material property determinations of two blocks of alluvium that were extensively tested at Sandia National Laboratories (SNL) Geomechanics laboratory. The alluvium blocks are intended to serve as surrogate material representative of that in situ to support the SPE dry alluvium geology (DAG) experimental series.

Five alluvium blocks were obtained from Area U1a and were originally collected to support new mining for the U1a Complex enhancements project (Geology & Geophysics Group, 2017). Three of the blocks were tested by an independent Geotechnical firm (Ninyo & Moore, 2017); coring/right circular cylinder fabrication by them was unsuccessful, and mechanical property tests were conducted on remolded material. The remaining two blocks were delivered to SNL for Geomechanical testing to support SPE. While not from Area 2 of NNSS, these blocks were deemed an acceptable surrogate to the DAG site, U2ez based on geologic description, water content, and density.

Strength measurements have been conducted on material from NNSS, Areas 2 and 1, (Kusubov et al, 1984, TerraTek, Inc., 1999). Kusubov performed unconfined and triaxial compression testing on U2ev alluvium samples that were dried and then rewetted by sealing samples in a plastic bag with a specific amount of water. Confining pressures for triaxial tests were limited to 10 MPa.

TerraTek performed unconfined and triaxial compression tests on U1a alluvium. Confining pressures were 3.4 MPa or less (one test at 5.2 MPa). The TerraTek samples were frozen and preparation (coring, cutting, and grinding) were performed after immersion in liquid nitrogen.

The downside to both testing methods is potential alteration to the in-situ moisture content; in one case, samples were dried then rewetted, in the other case samples were subjected to thermal loading and unloading by going through freeze and thaw cycles. Additionally, only a limited range of confining pressures were performed.

The objective of this work was to improve on previous test methods to develop a perhaps better data base for mechanical properties of alluvium by minimally altering the in-situ moisture content of the U1a alluvium blocks and test a sufficient range of confining pressures to establish a failure envelope that satisfies the lithostatic stress conditions encountered in the DAG test hole (U2ez).

Table 1-1 lists the alluvium samples collected at U1a.104 drift for this testing effort. The last two blocks were transported to SNL March 2018. Throughout the report, samples numbers containing "SM" and "BM" refer to sample numbers 092817-U1a.104-A and 092817-U1a.104-B, respectively.

Sample number	Approximate sample location	Approximate block size (ft)	U1a Map Unit
092717-U1a.104-A	U1a. 104 face at CS 3+60, 6 ft ACI	1.1 x 2.0 x 0.5	1 with a few lenses of 2 and beds of clean 1/granular 2
092717-U1a.104-B	U1a. 104 face at CS 3+60, 8.3 ft ACI	<1 x 1 x 1	Interbedded clean 1 and reddish 1
092717-U1a.104-C	U1a. 104 face at CS 3+60, 2.5 ft ACI		1 with caliche stringers
092817-U1a.104-A	U1a. 104 face at CS 3+63, 2.9 ft ACI	1.8 x 2.2 x 0.3-1	1 with caliche stringers
092817-U1a.104-B	U1a. 104 face at CS 3+63, 7.5 ft ACI	1.7 x 1.9 x 1-1.4	1 with beds of granular 2

Table 1-1. Alluvium samples collected at U1a. 104 Drift. The last two blocks (092817-U1a.104-A and 092817-U1a.104-B) were tested by Sandia National Laboratories.

2. SAMPLE PREPARATION

The blocks were received wrapped in multiple layers of plastic for protection during transport and to retain in-situ moisture (Figure 2-1). It was desirable to minimize a change in moisture during sample preparation. Because of the variable fragility between the two alluvium blocks, sample preparation for each block varied significantly.

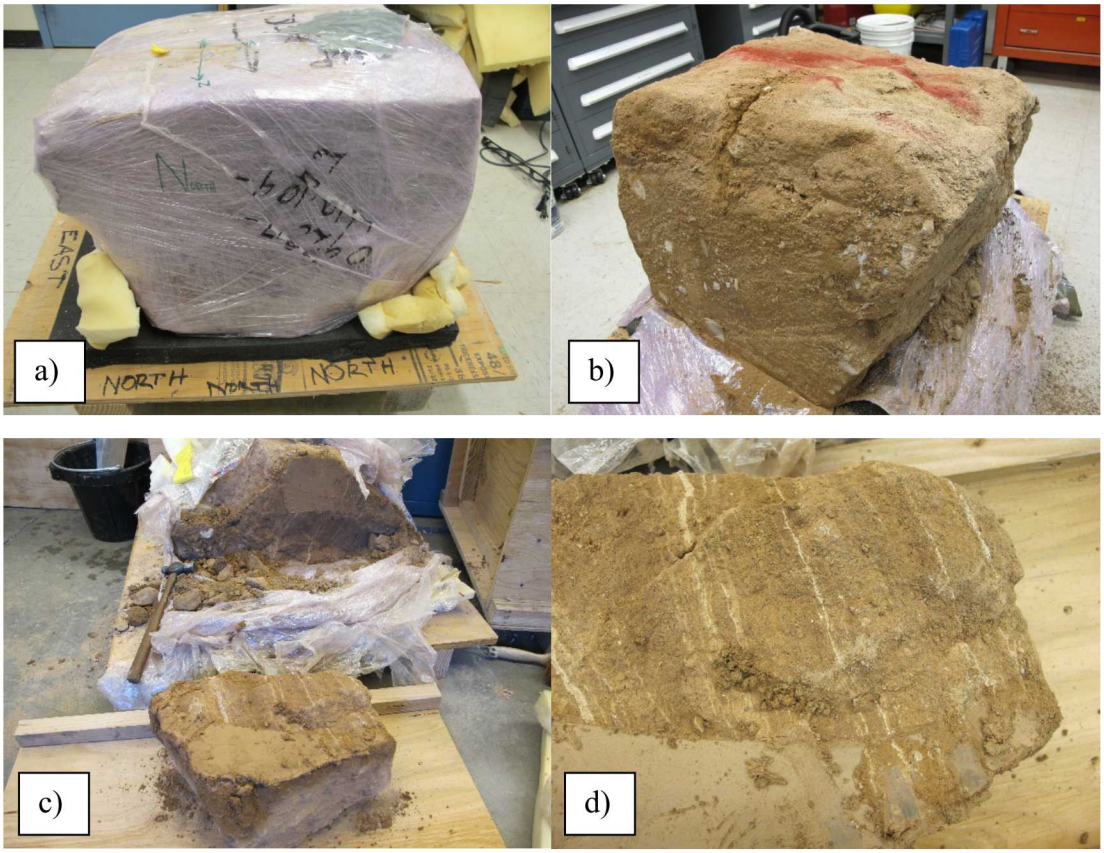

Figure 2-1. a) Block BM sealed in plastic wrap, b) unwrapped, c) block SM after extraction of large piece, and d) close up of extracted SM piece.

Samples from block SM were cored after the block was cut into smaller pieces. Multiple methods of coring were explored. The successful method was to use a two inch inside diameter segmented core bit dry and core rapidly at high speed to reduce the drying time of the alluvium. This both kept the moisture relatively stable and kept the alluvium from falling apart due to drying. Compressed air was used to clear the cuttings from the core bit. The resulting cores were quite smooth and were considered acceptable for strength testing purposes (Figure 2-2).

Figure 2-2. Two-inch diameter core drilled from block 092817-U1a.104-A.

Coring was attempted on block BM using the same method as on block SM but was unsuccessful. Block BM contains larger cobbles and is more friable than block SM. For block BM, it was decided to extract smaller pieces from the main block and then as shown in Figure 2-3, trim those pieces to rough size using a diamond wire saw. The trimmed pieces were then carefully clamped in a lathe and slowly rotated while a high-speed diamond grinding wheel was moved across the rotating sample (Figure 2-4). Each pass of the grinder initially took off approximately 0.025 inches of material. Approaching the target diameter, less material is taken off per pass (0.010 to 0.015 inches). As shown in Figure 2-5, the end result is a cylindrical sample within a few thousandths of an inch of the desired two-inch diameter.

Figure 2-3. BM sample cut to rough size on diamond wire saw prior to turning on a lathe.

Figure 2-4. BM sample turning on a lathe. The grinder moved horizontally to initially remove 0.025 inch per pass.

Figure 2-5. BM sample after turning on a lathe.

After a cylindrical shape was achieved for samples from both blocks, as shown in Figure 2-6, the ends were cut to length on the same diamond wire saw used to trim

down large pieces of BM material (Figure 2-3). Water was dripped on the diamond wire which kept the cutting surface wet and also kept the end piece from breaking off after the cut was finished.

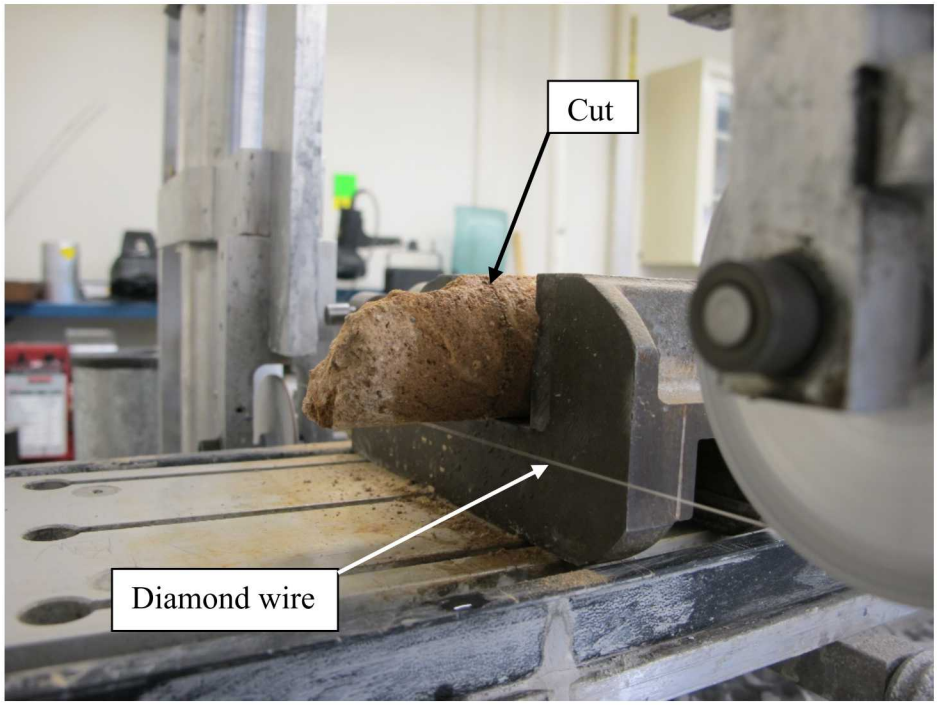

Figure 2-6. Wet cutting the end of a sample with a diamond wire saw.

After the final cutting operations were completed the sample was weighed and length and diameter measured. By assuming a right circular cylinder geometry, density was calculated. Brass buttons (custom fabricated at Sandia's Geomechanics laboratory) were glued to the sample to provide mounting points for radial displacement transducers. To protect the sample from confining fluid, a urethane jacket was applied and cured with UV light. The jacket also keeps the sample end caps located correctly and keeps the moisture content stable until the sample is tested. Unconfined Compressive Strength (UCS) samples were not jacketed because it was felt the jacket material may significantly increase the strength of the unconfined material; moisture content was maintained in UCS samples by keeping samples sealed in a plastic bag until testing.

Sample preparation on BM material required constant misting of water on the material; without frequent misting, the sample had a high likelihood of breaking. As a result, the moisture content of prepared BM samples was higher than the as received moisture content. To ensure measured triaxial strength was not affected by the additional moisture content, additional samples were tested that had been dried by leaving the prepared sample exposed to laboratory air with sufficient time such that the tested moisture content was similar to the in-situ moisture content.

This page is intentionally left blank.

3. EXPERIMENTAL METHODS

A test matrix was developed (Table 3-1) to determine on blocks SM and BM the compressional failure envelop, hydrostatic compaction (pore crush), elastic properties as a function of stress (bulk modulus versus mean stress, shear modulus versus shear stress, Young's modulus versus axial stress and Poisson's ratio versus axial stress), porosity and moisture content. All compressional tests were performed undrained.

Throughout this report stress and strain are plotted as true stress and true strain. "True" factors in the change of sample dimensions during deformation. Equation 1 gives true radial strain.

$$\varepsilon_L = -\mathrm{Ln}(\delta_D / I_D) \quad (1)$$

where ε_L is true lateral or radial strain, δ_D is current diameter, and I_D is initial diameter. True axial stress is the axial force divided by the current sample area.

U1a Alluvium block test matrix for SPE

Sample	Test	Quantity	Property
092817-U1a. 104-A	UCS	2	Young's modulus, Poisson's ratio, Unconfined compressive strength
092817-U1a. 104-A	5 MPa CMS	2	Shear modulus, confined compressive strength
092817-U1a. 104-A	10 MPa CMS	3	Shear modulus, confined compressive strength
092817-U1a. 104-A	20 MPa CMS	2	Shear modulus, confined compressive strength
092817-U1a. 104-A	300 MPa Hydrostatic	2	Bulk modulus, pressure/volume relationship, pore crush
092817-U1a. 104-B	UCS	2	Young's modulus, Poisson's ratio, Unconfined compressive strength
092817-U1a. 104-B	5 MPa CMS	2	Shear modulus, confined compressive strength
092817-U1a. 104-B	10 MPa CMS	3	Shear modulus, confined compressive strength
092817-U1a. 104-B	20 MPa CMS	2	Shear modulus, confined compressive strength
092817-U1a. 104-B	300 MPa Hydrostatic	2	Bulk modulus, pressure/volume relationship, pore crush
	Total tests	22	

Note: All hydrostatic and triaxial (CMS) tests performed undrained

Table 3-1. Test matrix developed for alluvium blocks SM and BM (092817-U1a.104-A and 092817-U1a.104-B).

3.1. Constant Mean Stress tests

To create a compressional failure envelope within the stresses of interest to DAG and measure shear modulus, constant mean stress (CMS) tests under a triaxial stress condition were performed. On all triaxial tests, the three principal stresses as well as axial and radial strains were measured. Volume strain was calculated from:

$$\varepsilon_V=\varepsilon_A+2*\varepsilon_L \quad (2)$$

where ε_A is axial strain and ε_L is lateral (radial) strain. There were four tests performed with constant confining pressure of zero (uniaxial compression) and the remaining tests were performed under CMS conditions. For a CMS triaxial test, the initial hydrostatic stage is increased to the target pressure and then during axial loading the confining pressure is decreased so that the average of the three principal stresses remains constant. With a right circular cylinder geometry, the confining (stress) pressure is decreased by half the amount that the differential stress is increased. CMS stress state allows direct measurement of shear modulus while uniaxial compression provided direct measurement of Young's modulus and Poisson's ratio. Throughout the test, multiple unload/reload cycles were performed. The aforementioned elastic properties are determined from the unload slope during the unload/reload loop. All triaxial tests were conducted at $5E^{-05}$/s axial strain rate. In some cases, samples may shorten axially in excess of 25%; samples are tested using a constant displacement rate and thus the starting axial strain rate will slightly increase during the test. Figure 3-1 shows a triaxial sample instrumented with displacement transducers for measuring axial and radial displacements. Radial gauges are mounted on short brass buttons that are glued to the sample and axial displacement transducers are attached to steel endcaps. The displacement from the steel endcaps is insignificant compared to sample displacement.

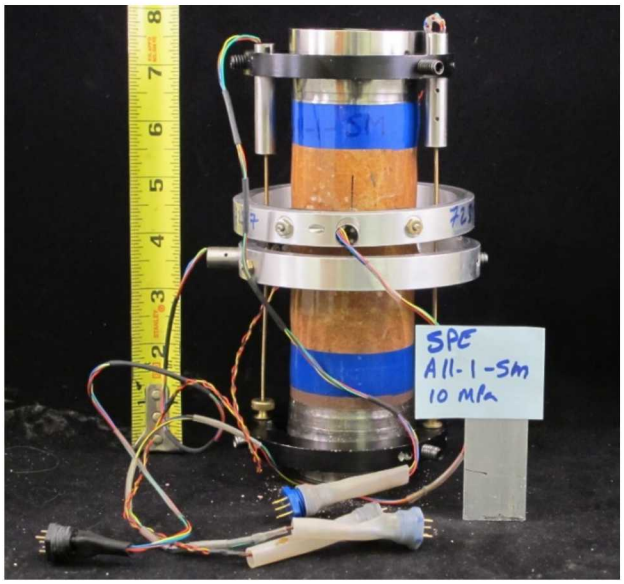

Figure 3-1. Sample instrumented with displacement transducers for determination of axial and radial strains.

3.2. Hydrostatic tests

Dedicated hydrostatic tests were performed up to a maximum of 400MPa confining pressure. Three principal stresses as well as axial and radial strains were measured; volume strain was calculated from Equation (2). The beginning stage (pressurization up to target confining pressure) of each triaxial test is also a hydrostatic test. Hydrostatic tests are plotted as pressure versus volume strain. Initially, at low pressures, the pressure vs. volume strain curve is less steep, indicating open cracks and sample compliance (Walsh, 1982). When cracks close, the slope becomes steeper until pore crush begins at which point a decrease in the slope of the curve is observed. The point when pore crush begins is considered the onset of pore crush and is reported for all hydrostatic tests (including triaxial tests). Mathematically, the onset of pore crush is determined from pressure versus volume strain curves where the slope starts to trend toward zero or becomes less steep. Walsh, 1982 states a rule of thumb where the effect of cracks on elastic properties depends on the total surface area of the crack phase where the effect of pores is in direct proportion to the volume of the pore phase. The alluvium tested here is sufficiently weak and pore volume is plastically reduced at a relatively low hydrostatic pressure.

3.3. Porosity

Porosity was measured using a helium porosimeter following Jones and Associates, 1985 on three samples each from blocks SM and BM. Accuracy of this method relies on careful system calibration and measured sample density. Samples were right circular cylinders nominally 1.5 inches diameter and either one or two inches in length. Both wet and dry porosity measurements were obtained. Wet porosity performs as a secondary indicator of sample moisture content. Figure 3-2 shows porosity samples from block SM and the helium porosimeter.

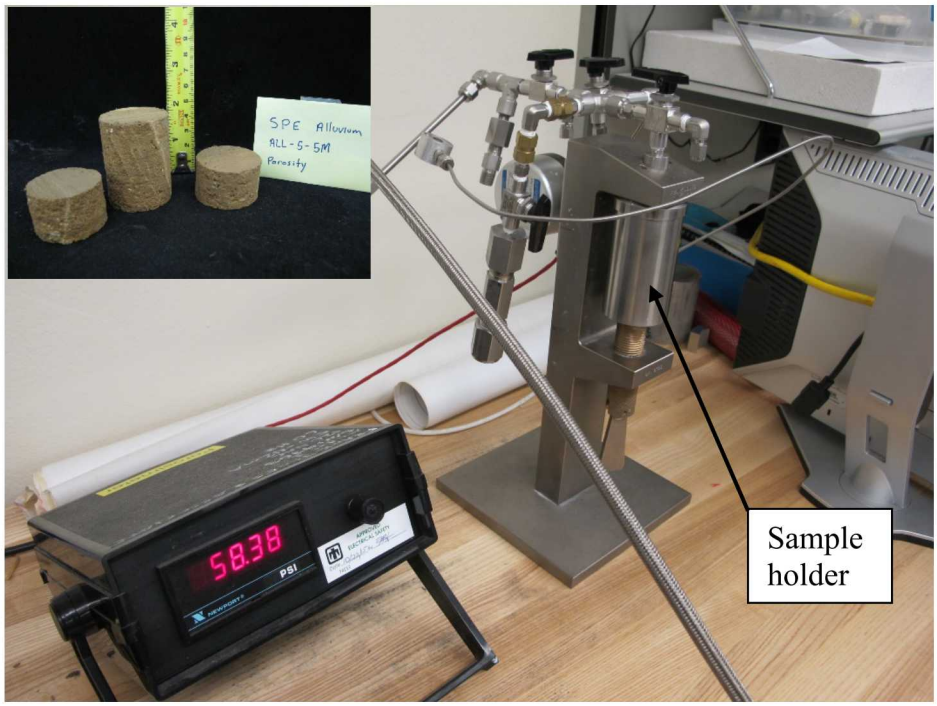

Figure 3-2. Porosity samples from block SM (upper left) and helium porosimeter.

3.4. P- and S-Wave Velocity

Ultrasonic compressional and shear wave velocity measurements were conducted on two samples from each block. Figure 3-3 shows a typical voltage versus time plot used to determine P-and S-wave velocities.

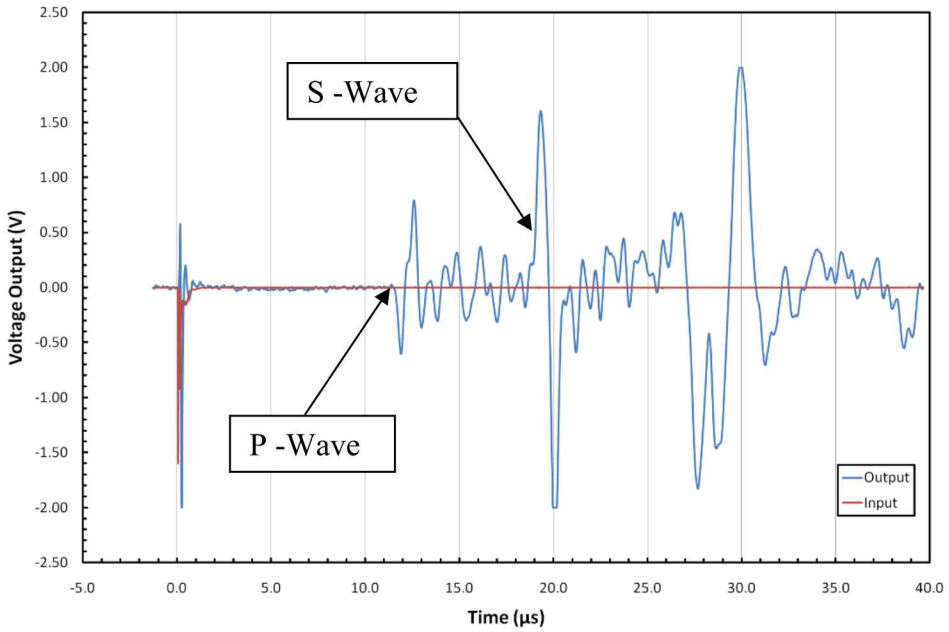

Figure 3-3. Typical velocity profile for determination of P & S wave speed.

The dynamic elastic Young's modulus, (E), was determined directly from:

$$E_{dynamic} = \frac{\rho V_S^2 \left(3V_P^2 - 4V_S^2\right)}{\left(V_P^2 - V_S^2\right)} \tag{3}$$

Where ρ is the sample density and V_P and V_S are the compressional and shear wave velocities, respectively. The dynamic elastic Poisson's ratio, $\nu_{dynamic}$, was calculated from:

$$\nu_{dynamic} = \frac{\left(V_P^2 - 2V_S^2\right)}{2\left(V_P^2 - V_S^2\right)} \tag{4}$$

4. RESULTS AND DISCUSSION

4.1. Constant mean stress tests

Seventeen CMS tests under a triaxial stress condition were performed. Two tests on each block were UCS (confining pressure equals zero). Pressure versus strain and stress versus strain plots for each CMS test and stress versus strain plots for each UCS test are listed in Appendix A. The UCS for the BM and SM is in the range of 0.5-0.6, and 2.0-2.6 MPa respectively. From Kandolkar et al, 2012, the UCS of a tamped soil with 11.2% moisture content is 0.3 MPa or about half the strength of the BM material.

A typical stress versus strain plot is shown in Figure 4-1. The failure point of a test is when peak axial stress occurs. If the axial stress continues to gradually climb (as seen in Figure 4-1), then the highest axial stress value (also the point of maximum axial strain) is chosen for the failure point. Figure 4-2 shows compressional failure envelopes for blocks SM and BM. The data are plotted in true differential stress versus true mean normal stress space.

Polynomial fits were chosen because of the accuracy of the fit to the data within the range of stresses tested. Samples intentionally dried out to represent the in-situ moisture content from block BM are represented by green data points. All BM failure points, including the moist samples, are plotted in red. SM is plotted in blue. In all cases strength increases with increasing normal stress.

For the BM, moisture content changes the failure surface, moisture content closer to as- received appears to strengthen the material and the change is most significant at higher confining pressures. One explanation for the weaker strength in the wetter BM material at higher confining pressures could be pore pressure. At higher confining pressures (>10 MPa), the material has begun to significantly crush up (greater volume strain) during hydrostatic compaction. With additional axial compaction during the CMS stage of the test, there could be anomalous pore pressure which would reduce the effective confining pressure resulting in a lower peak differential stress.

There is only one data point at each confining pressure for the drier samples. Therefore, generalizations on the role of moisture in failure strength for BM material should be limited. From Figure 4-2, block SM has higher cohesion (y-intercept) than block BM. Both blocks have a similar compressional failure surface up to a mean normal stress level of approximately 8 MPa. Block BM is significantly weaker for mean normal stress levels above 8 MPa.

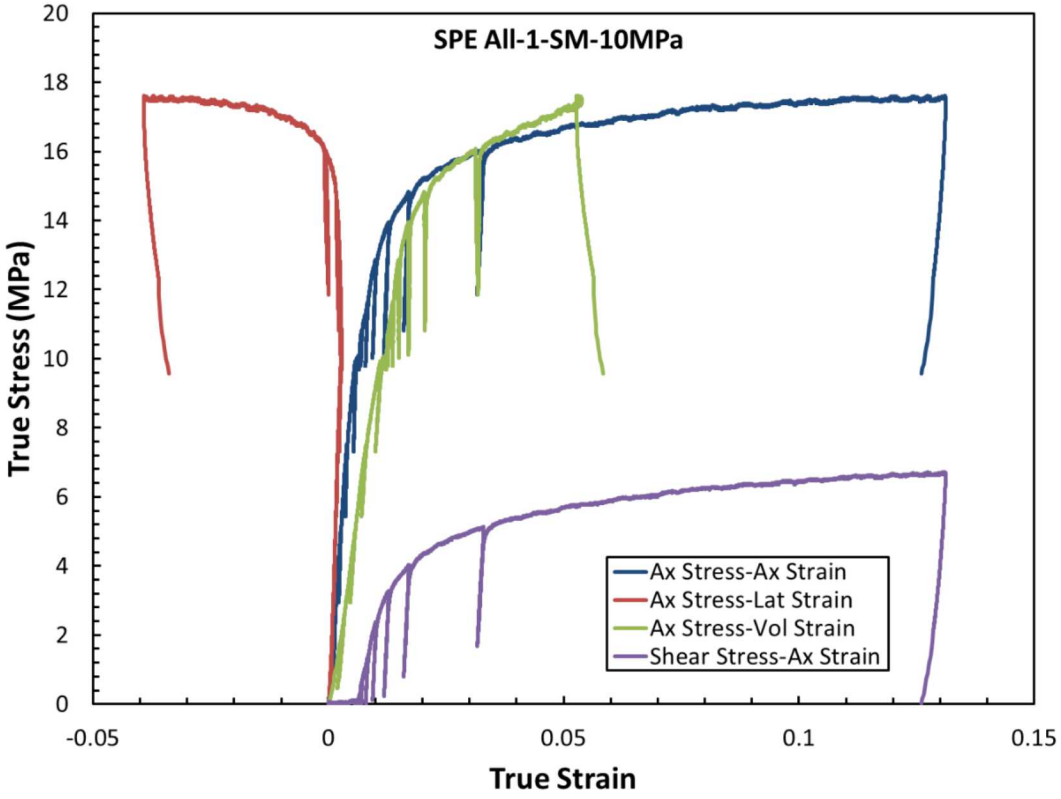

Figure 4-1. Typical stress versus strain plot for block SM.

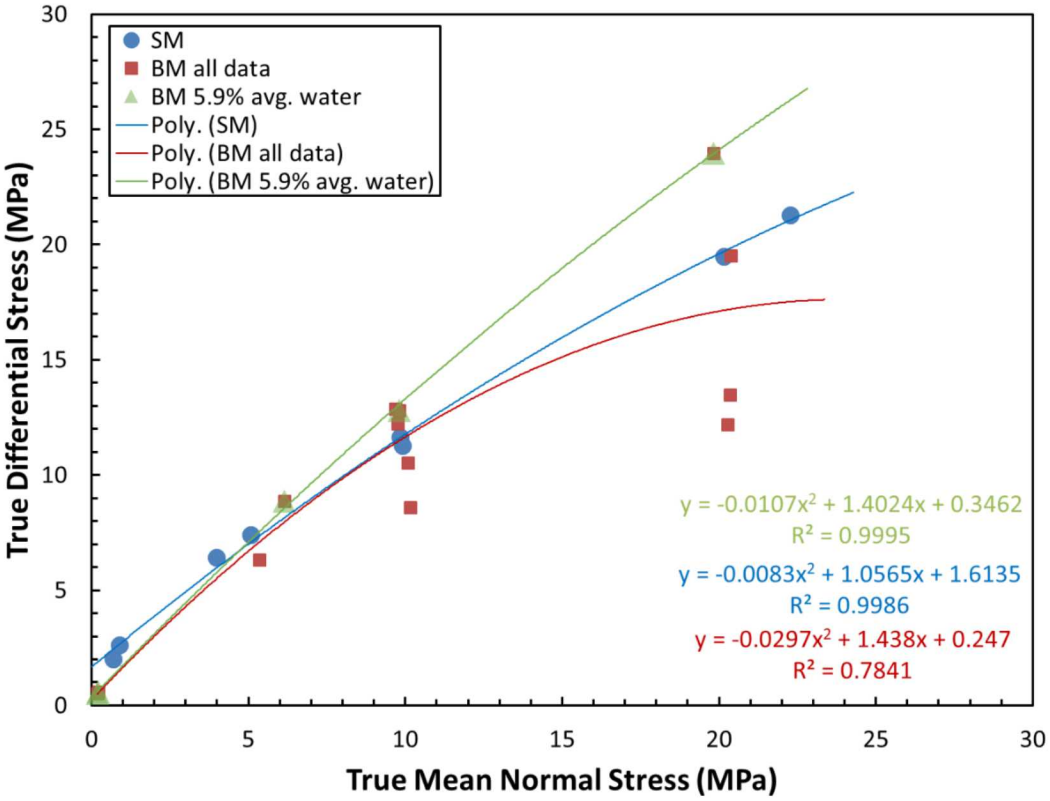

Figure 4-2. Compressional failure envelopes for blocks SM and BM.

4.2. Hydrostatic tests

Four dedicated hydrostatic tests were conducted; two on each block. The pressure versus volume response of the four hydrostatic samples is shown in Figure 4-3. True volume strain is calculated from Equation 1 and factors in the change of length and diameter during compaction. For one sample from each block a test was performed monotonically (i.e. without unload/reload loops). Unload/reload loops for sample SPE-All-09-SM-300MPa were conducted during crush up of the material. Following the last unload/reload loop, the material significantly stiffened. Because of this, it was decided to perform unload/reload loops after crush up occurred in sample SPE-All-10-BM-300MPa to determine the potential impact of pressure loops upon the crush up stage of the test. Sample SPE-All-10-BM-300MPa behaved in a similar manner to SPE-All-09-SM-300MPa in that a distinct inflection point is observed (around 15% volume strain) and may indicate full saturation of pores with water. This is a typical compaction plot for an undrained condition. The stiffness after the inflection point may show the compressibility of the grains of the sample. The distinct inflection point for both of these samples (SPE-All-09-SM-300MPa and SPE-All-10-SM-300MPa) is likely not related to where unload/reload loops were conducted.

Samples from block SM had similar total volume strain and test densities of approximately 22% and 1.8 g/cc, respectively. BM samples yielded 18% (tested density of 1.90 g/cc and moisture content of 12.6%) and 37% (tested density of 1.58 g/cc) total volume strain. The wide variation in total volume strain between the BM

samples is likely due to moisture level which may be inferred from density (tested moisture level is not available for SPE-All-02-BM-400MPa). In Appendix B, pressure versus strain plots are given for each hydrostatic test.

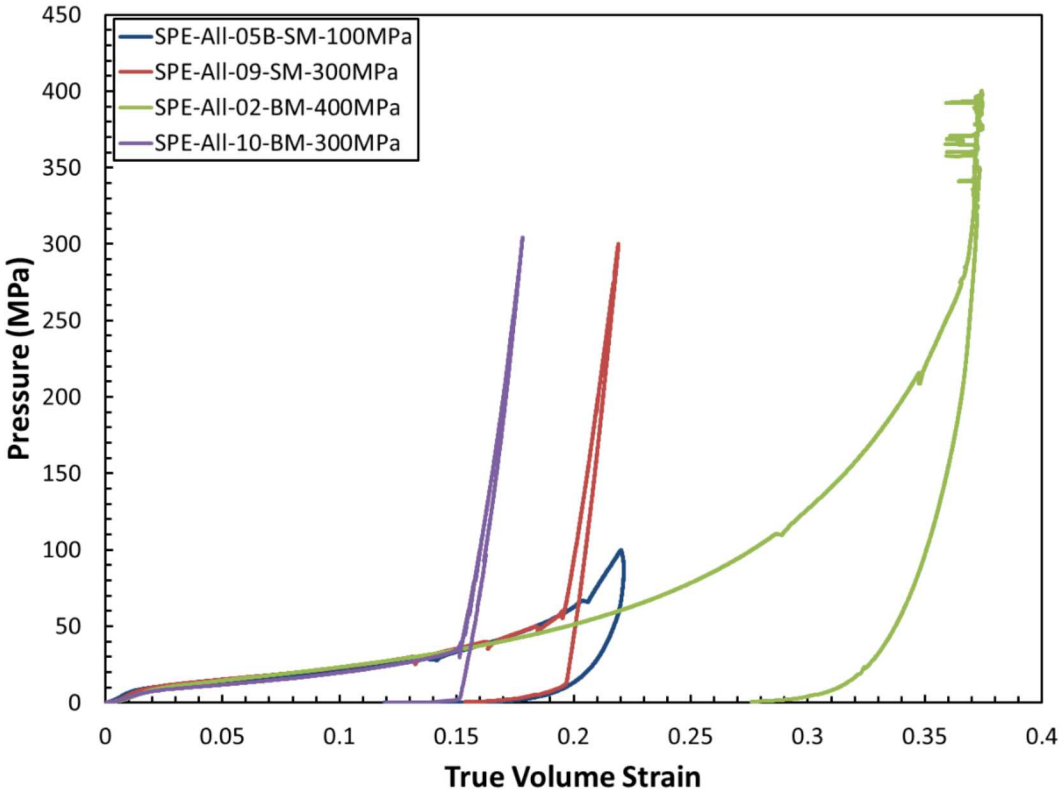

Figure 4-3. Pressure versus true volume strain for blocks SM and BM.

4.3. Porosity

Porosity was determined for both wet (near in-situ moisture) and dried samples (Table 4.1). Most of the moisture levels are about 3-5% higher than the in-situ measured moisture and is a result of sample preparation techniques necessary to prepare testable samples. Samples from both blocks of rock all have porosities in the range of 35-40% when dry. This implies that the alluvium was never consolidated, or buried by greater overburden, beyond its current state; 35-40% is a common bulking value.

Block/Sample #	Porosity (%) (wet/dry)	Moisture Content (%)	Density (g/cc)
092817-U1a. 104-A/SM			
All-5-SM-P1	13.5/38.6	13.8	1.81
All-5-SM-P2	13.6/36.5	12.9	1.86
All-5-SM-P3	13.0/35.9	12.7	1.87
092817-U1a. 104-B/BM			
All-BM-P1	N/A/38.9	8.7	1.55*
All-BM-P2	17.6/38.2	12.2	1.77
All-BM-P3	10.2/36.6	14.5	1.89

*Dry density, all others are wet densitiy.

Table 4-1. Porosity measured on samples from blocks SM and BM.

4.4. P- and S-Wave Velocity and Summary of Strength and Elastic Properties

Density was determined on P- and S-Wave samples from known geometry and weight. Sample All-1-BM-1A was irregular in shape and the average effective diameter was not easily determined. The uncertainty in diameter resulted in an unrealistic density for this sample. Because $E_{dynamic}$ is dependent on density, it was decided to use an adjacent sample density for calculation of $E_{dynamic}$ for this sample.

Tables 4-2 and 4-3 list average elastic properties for each sample, onset of pore crush, moisture content, peak differential stress and mean stress at peak differential stress. Due to the mechanics of performing CMS mode triaxial testing, the mean stress value for CMS triaxial tests is close to the confining pressure prior to increase in differential stress. For UCS tests the mean stress value is 1/3 of the peak differential stress because $\sigma_2=\sigma_3=0$. Moisture content was determined from oven drying samples at approximately 60°C until they no longer lost weight (typically between 1 and 5 days).

Figures 4-4 and 4-5 show elastic properties plotted as bulk modulus versus pressure and shear modulus versus shear stress. On Figure 4-6, the primary Y axis plots Young's modulus versus axial stress and the secondary Y axis plots Poisson's ratio. In nearly all cases, bulk modulus increases with increasing confining pressure. For the two hydrostatic tests where unload/reload loops were conducted, bulk modulus over 20 MPa pressure can be seen to increase up to 60 MPa pressure for block SM. Compared to block SM, block BM does not exhibit a significant increase in bulk modulus between 40 MPa and 100 MPa confining pressure. From Figure 4-5, shear modulus decreases with increasing shear stress up to a value of approximately 4 MPa where shear modulus remains relatively constant..

Because UCS of block BM is much lower than block SM, Young's modulus and Poisson's ratio was measured up to 0.5 MPa axial stress for block BM and up to nearly 2.0 MPa axial stress for block SM. Young's modulus increases with increasing axial stress for both blocks. Poisson's ratio is higher (0.24 compared to 0.49) for block BM. Block SM Poisson's ratio ranges from 0.08 to 0.2.

Block/Sample #									
092817-U1a. 104-A/SM	Avg. Young's Modulus (MPa)	Avg. Poisson's Ratio	Avg. Bulk Modulus (GPa)	Avg. Shear Modulus (GPa)	Onset of pore crush (MPa)	Moisture Content (%)	Peak Differential Stress (MPa)	Mean Stress at Peak Diff. Stress (MPa)	Density (g/cc)
SPE-All-1-SM-10MPa			1.8	1.7	2.6		11.6	9.8	1.88
SPE-All-2-SM-20MPa			1.7	2.0	3.6		19.5	20.1	1.84
SPE-All-3-SM-20MPa			1.6	2.1	2.8		21.3	22.3	1.86
SPE-All-4-SM-10MPa			2.2	1.6	3.2		11.3	9.9	1.84
SPE-All-5-SM-0MPa	1064	0.15					2.0	0.7	1.83
SPE-All-6-SM-0MPa	1301	0.12					2.6	0.9	1.82
SPE-All-7-SM-5MPa			1.5	1.7	2.7		7.4	5.1	1.86
SPE-All-8-SM-5MPa			1.5	1.9	2.4		6.4	4.0	1.81
SPE-All-5B-SM-100MPa					3.5				1.77
SPE-All-9-SM-300MPa			8.7		3.7				1.80
All-SM-MS-A						8.8			
All-SM-MS-O						8.9			
	P-wave (m/s)	S-wave (m/s)	E dynamic (GPa)	v dynamic					
All-10-SM-A	1834	1042	4.82	0.26					1.76
All-10-SM-B	1924	905	4.18	0.36					1.88

Table 4-2. Modulus, pore crush, moisture, strength, P-&S-wave velocity, and density summary from block SM.

092817-U1a. 104-B/BM	Avg. Young's Modulus (MPa)	Avg. Poisson's Ratio	Avg. Bulk Modulus (GPa)	Avg. Shear Modulus (GPa)	Onset of pore crush (MPa)	Moisture Content (%)	Peak Differential Stress (MPa)	Mean Stress at Peak Diff. Stress (MPa)	Density (g/cc)
All-BM-MS-1						6.8			
All-BM-MS-2						8.4			
All-BM-MS-3						5.2			
SPE-All-01-BM-0MPa	349	0.4				7.5	0.5	0.2	1.74
SPE-All-02-BM-400MPa					4.8				1.58
SPE-All-03-BM-5MPa			1.4	1.9#	4.4	4.7	8.9	6.1	1.87
SPE-All-04-BM-5MPa			1.0	1.4	4.8	15.3	6.3	5.3	1.95
SPE-All-05-BM-10MPa			1.4	1.4	5.1	14.5	10.5	10.1	1.88
SPE-All-06-BM-10MPa			1.2	1.3	4.4	14.5	8.6	10.1	1.91
SPE-All-07-BM-10MPa			1.6	1.8	4.7	10.3	12.9	9.7	1.94
SPE-All-08-BM-20MPa			2.0	2.2	4.2	12.9	12.2	20.3	1.92
SPE-All-09-BM-20MPa			1.9	1.9	3.9	12.8	13.5	20.4	1.91
SPE-All-10-BM-300MPa			10.5		2.3	12.6			1.90
SPE-All-11-BM-0MPa	420	0.31				5.9	0.6	0.2	1.79+
SPE-All-13-BM-10MPa			1.2	1.5	3.5	11.6	12.2	9.8	1.84
SPE-All-14-BM-20MPa			2.0	2.0	3.5	13.4	19.5	20.4	1.74
SPE-All-15-BM-20MPa			1.7	2.3	2.7	4.7	24.0	19.8	1.76
SPE-All-16-BM-10MPa			1.3	1.4	3.0	6.8	12.8	9.8	1.78
	P-wave (m/s)	S-wave (m/s)	E dynamic (GPa)	v dynamic					
All-1-BM-1A	1262	691	1.54*	0.29					1.25*
All-1-BM-2A	1252	530	1.38	0.39					1.76

*Diameter of sample estimated yielding unrealistic density; $E_{dynamic}$ is dependent on density
+Density calculated before air drying; as tested density unavailable
#Shear modulus estimated. CMS mode was calculated incorrectly resulting in slight change of mean stress during unload/reload loop

Table 4-3. Modulus, pore crush, moisture, strength, P-&S-wave velocity, and density summary from block BM

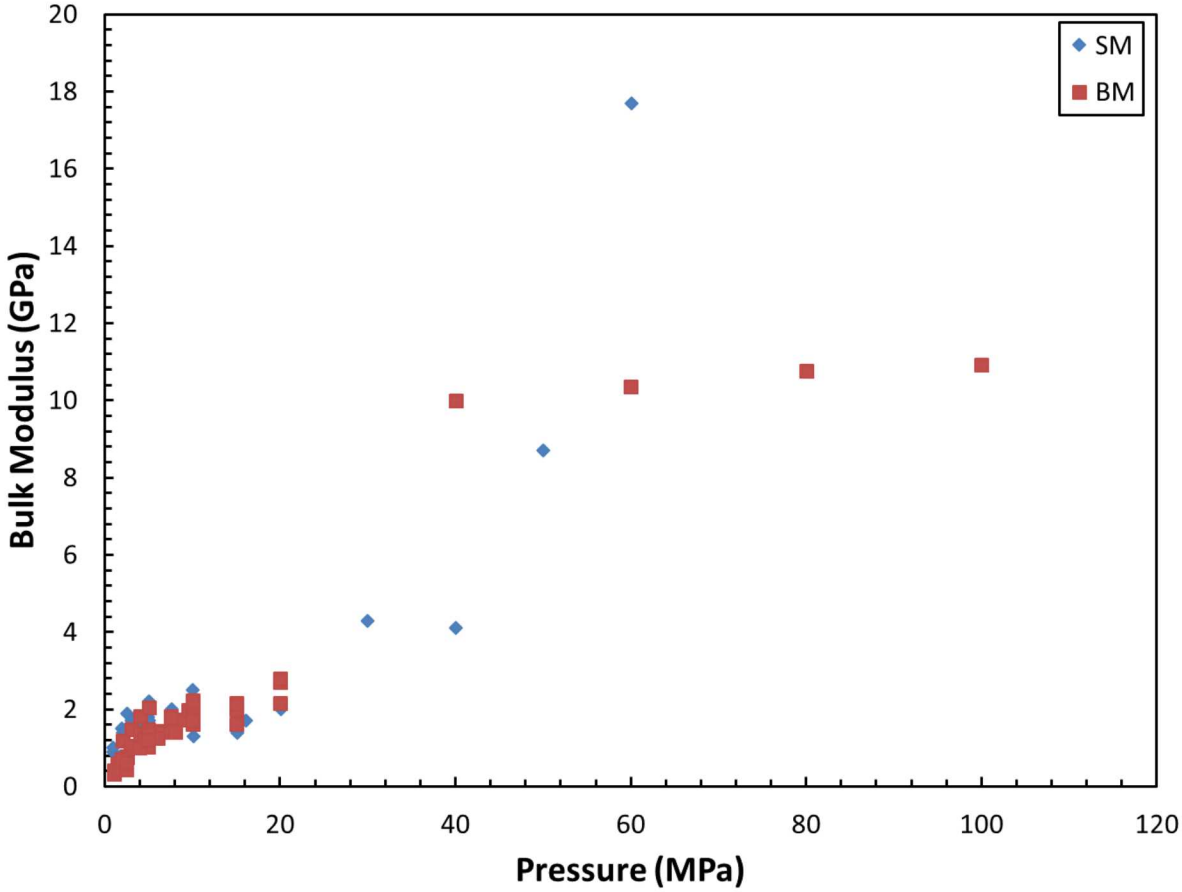

Figure 4-4. Bulk modulus versus pressure for blocks SM and BM.

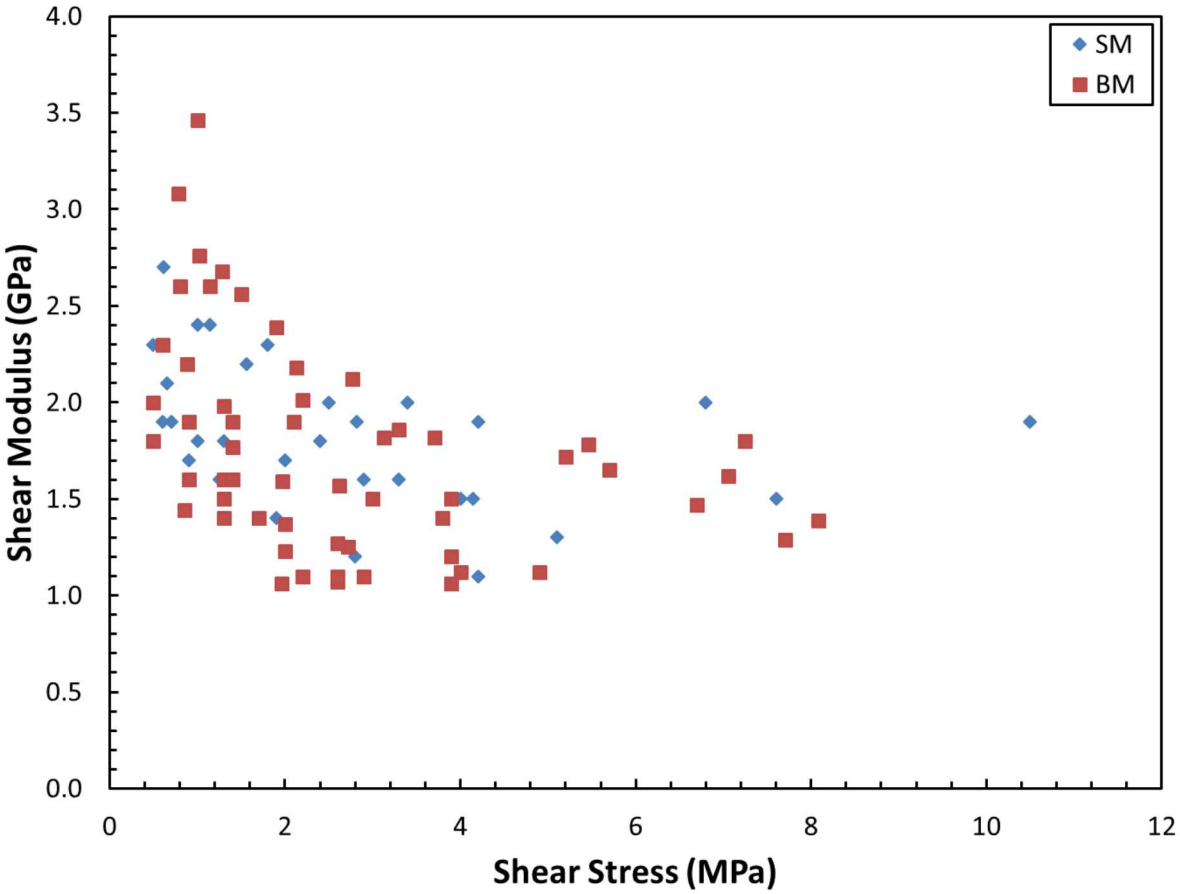

Figure 4-5. Shear modulus versus shear stress for blocks SM and BM.

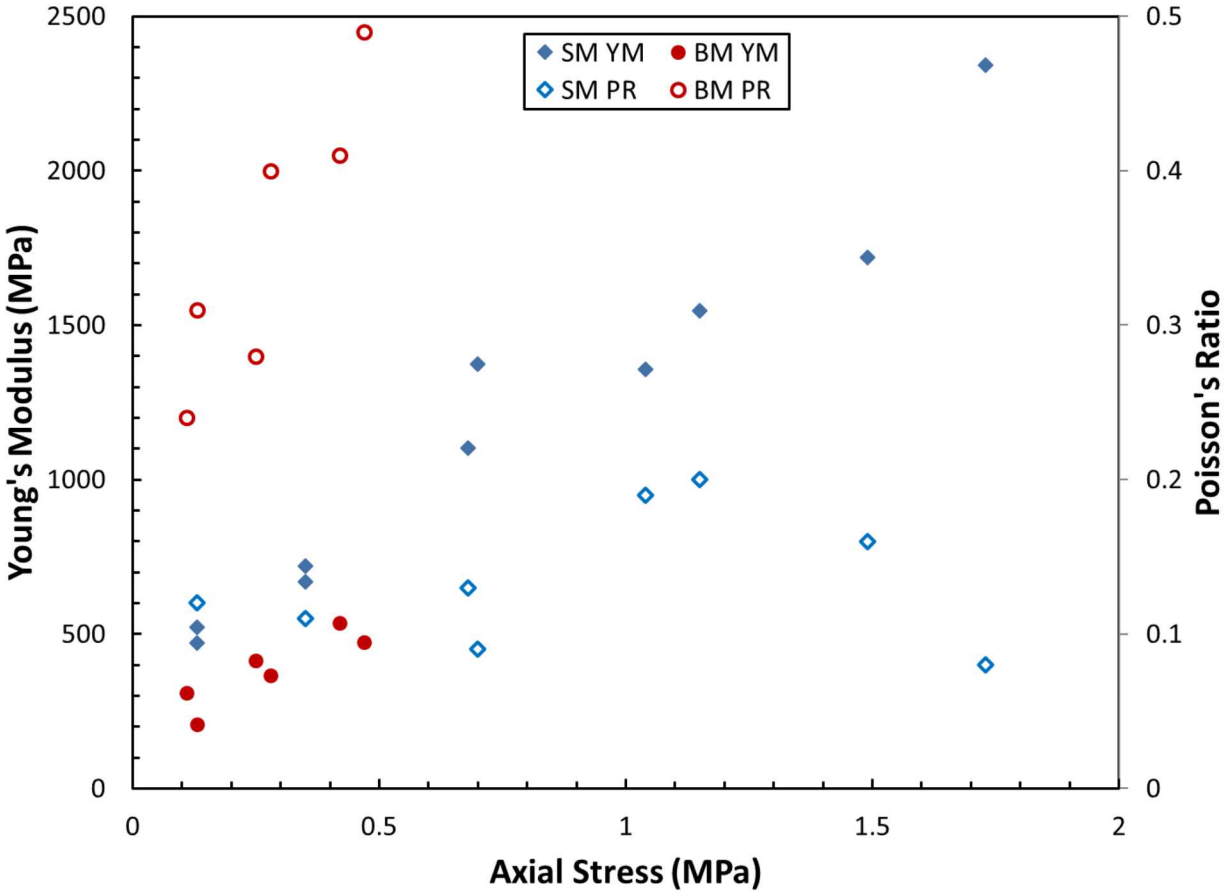

Figure 4-6. Young's modulus and Poisson's ratio versus axial stress for blocks SM and BM.

5. CONCLUSIONS

Two blocks of alluvium from Area U1a of NNSS were extensively tested at the Sandia National Laboratories Geomechanics Laboratory to determine the mechanical response to compressional loading under quasi-static conditions. These alluvium blocks are intended to serve as surrogate material to improve predictive model response of Area U2ez, the site of the SPE DAG experimental series.

A set of procedures were developed to assure preservation of the as-received moisture content for each block; slight deviation of moisture content resulted from sample preparation techniques and the effect of moisture variation on material properties is observed. It appears that the presence of moisture is reflected in the strength versus normal stress response; tests conducted at what are believed to be "average" in situ moisture contents are stronger than wetter conditions. This may have implications of test timing relative to rain and/or atmospheric conditions.

Tests conducted on each block included P-&S-wave velocity, triaxial compression, hydrostatic compression, and porosity. Samples from both blocks of rock all have porosities in the range of 35-40% when dry. From these measurements, material properties were determined including elastic properties (Young's modulus, Poisson's ratio, bulk modulus, shear modulus), unconfined compressive strength, confined compressive strength, pressure/volume response, and pore crush pressure. Generally, both Young's modulus and Poisson's ratio increase with increasing axial stress, bulk modulus increases with increasing pressure, and increases more dramatically upon pore crush, shear modulus decreases with increasing shear stress and then appears to plateau. The UCS for the BM is in the range of 0.5-0.6, and for SM in the range of 2.0-2.6 MPa. The confined compressive strength increases with increasing confining pressure and for each alluvium block, these data have been parameterized and failure envelops are presented. The BM alluvium is significantly weaker for mean stress levels above 8 MPa.

6. WORKS CITED

Geology & Geophysics Group. 2017 “Collection of Alluvium Blocks at U1a for Geotechnical Evaluation” National Security Technologies, LLC.

Ninyo & Moore. 2017 Test Results; Consolidated Triaxial Test Data Sheets.

Kusubov A. and Anderson G. 1984. “Interim Report on Strength Measurements on Material From Auger – Exploratory Hole UE2ev” *Interdepartmental Letter*. Lawrence Livermore National Laboratory.

TerraTek, Inc. 1999 “Mechanical Testing of Alluvium Samples for U1a Complex” TerraTek report. Prepared for Bechtel Nevada.

Walsh, J. 1982 “Deformation and Fracture of Rock.” National Research Council. *Conservation of Historic Stone Buildings and Monuments*. Washington, DC: The National Academies Press. doi: 10.17226/514.

Jones, F and Associates, Inc. 1985 “Porosimeter Theory” Theory of operation of Coberly-Stevens porosimeter.

Kandolkar, S. and Mandal, J. 2012. “Behavior of Mine Waste as Reinforced Soil” International Journal of Research in Engineering and Technology, Vol 1, Issue 2, pp. 82-89.

This page is intentionally left blank.

APPENDIX A: PRESSURE AND STRESS VERSUS STRAIN PLOTS FOR TRIAXIAL TESTS

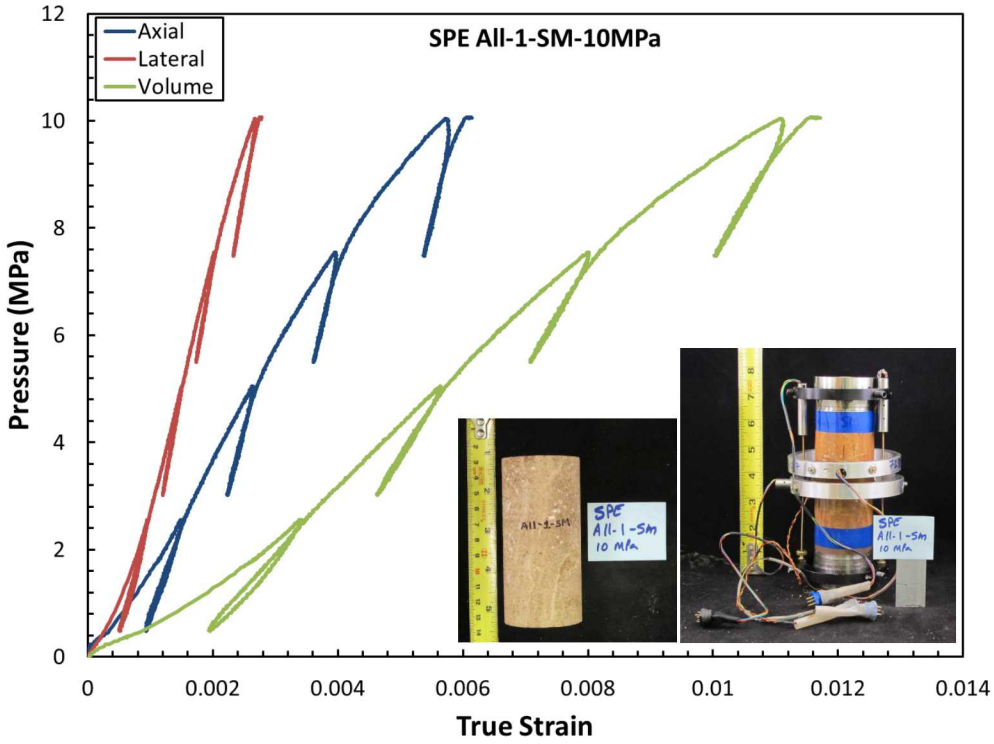

Figure A-1: Pressure versus strain plot for SPE All-1-SM-10MPa.

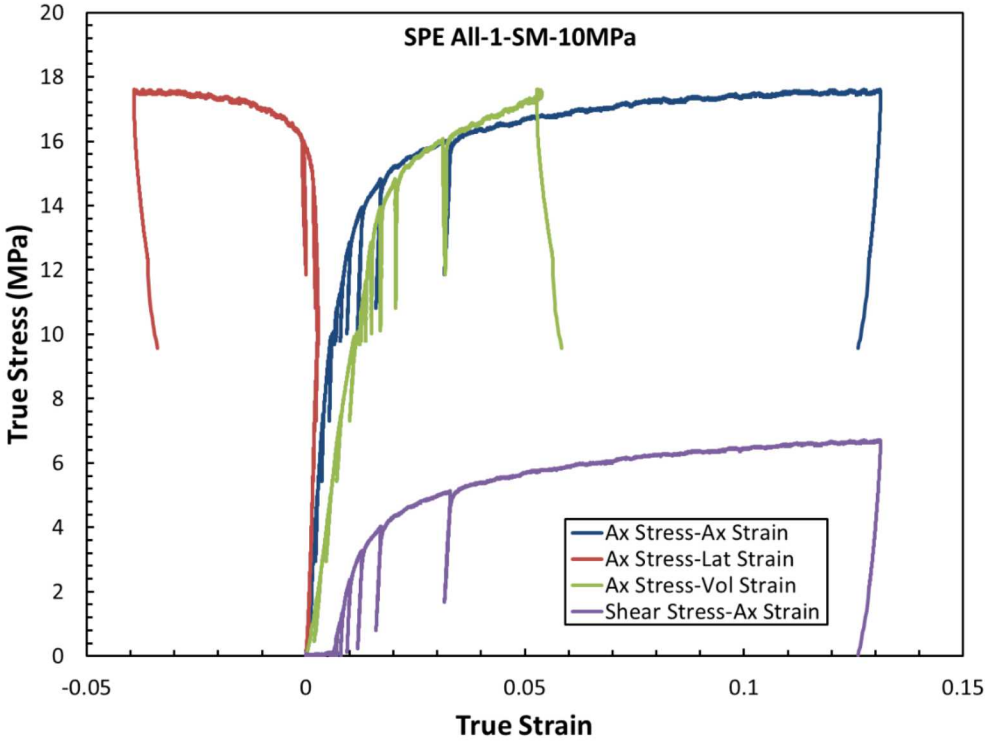

Figure A-2: Stress versus strain plot for SPE All-1-SM-10MPa.

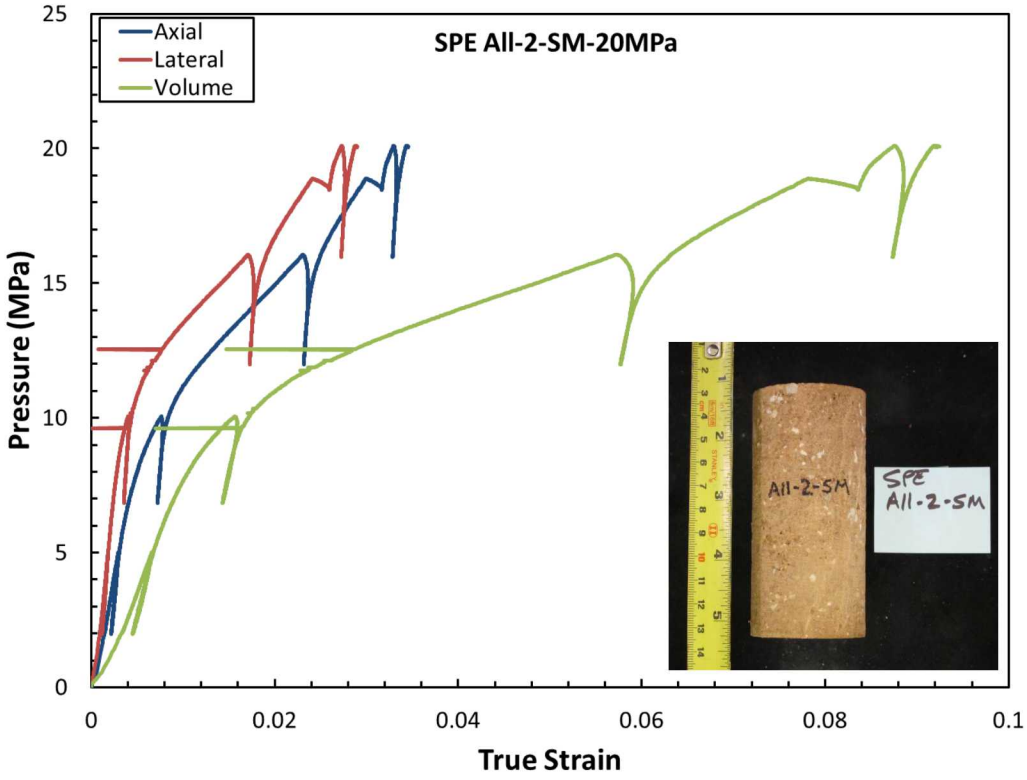

Figure A-3: Pressure versus strain plot for SPE All-2-SM-20MPa.

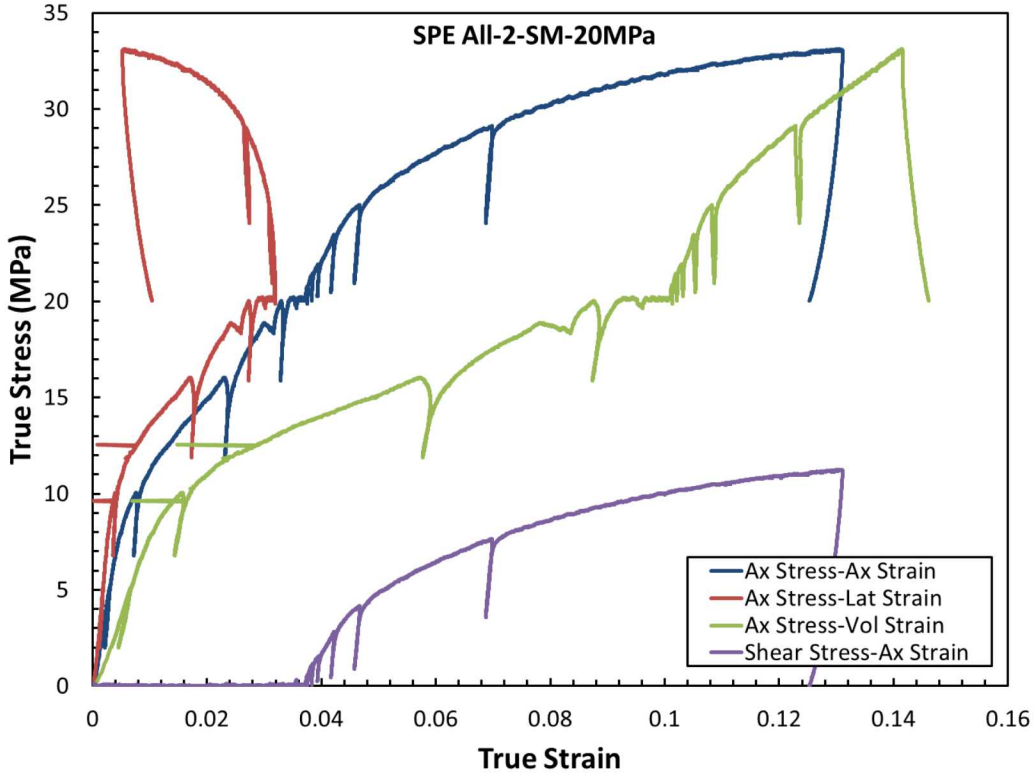

Figure A-4: Stress versus strain plot for SPE All-2-SM-20MPa.

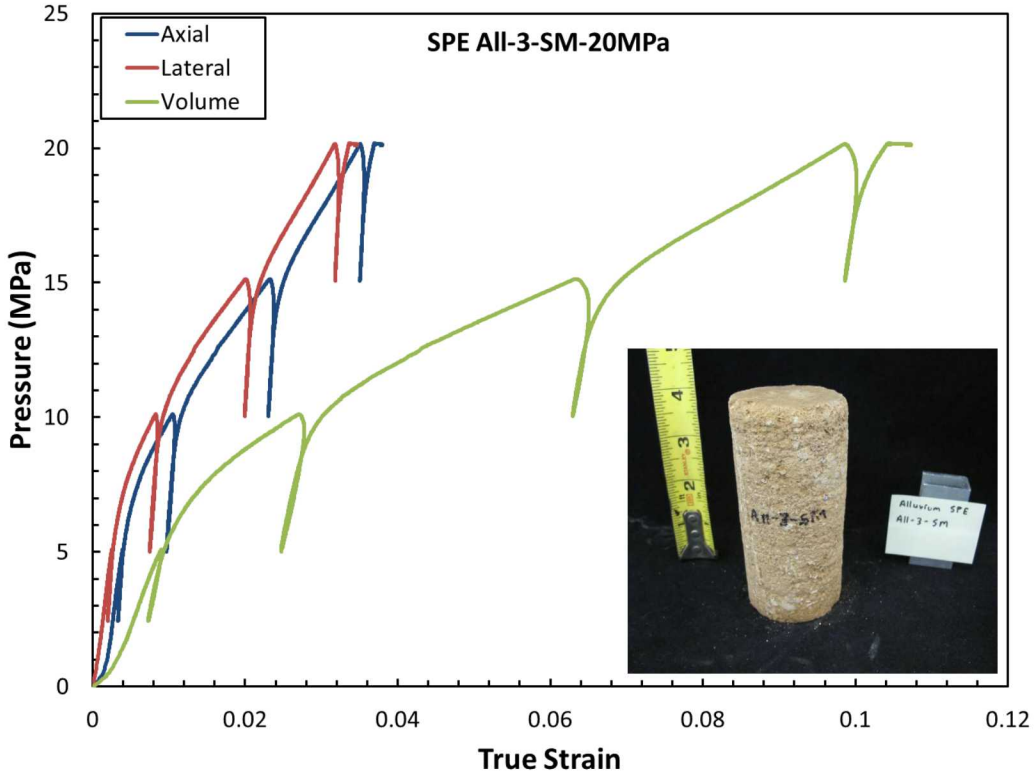

Figure A-5: Pressure versus strain plot for SPE All-3-SM-20MPa.

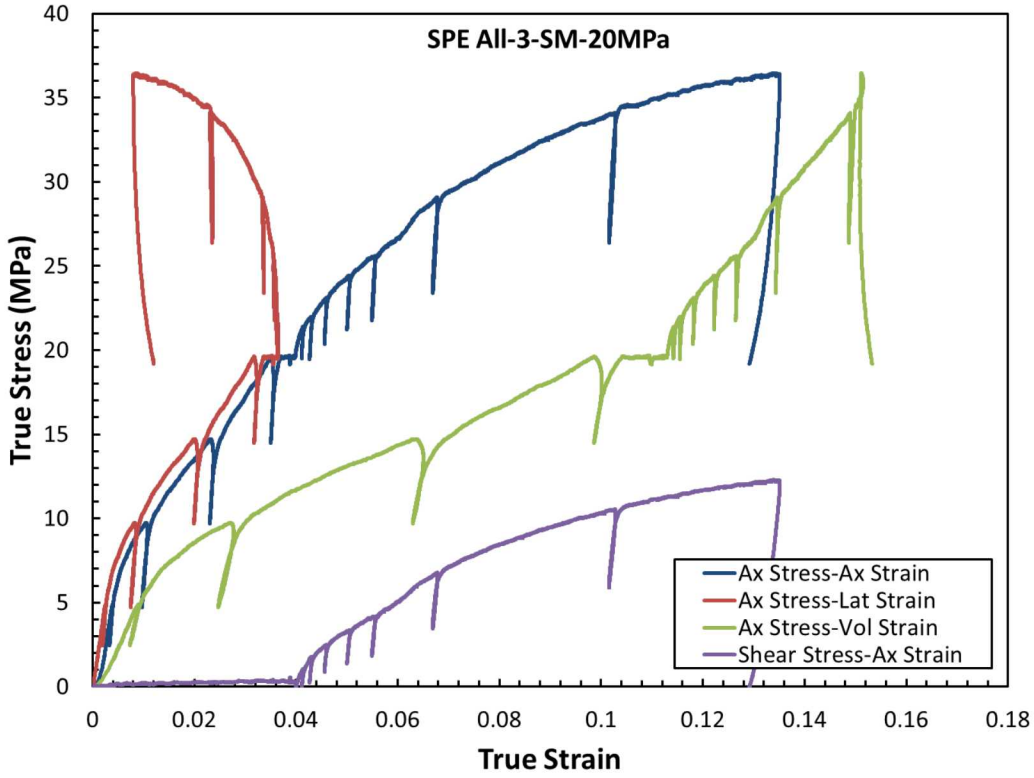

Figure A-6: Stress versus strain plot for SPE All-3-SM-20MPa.

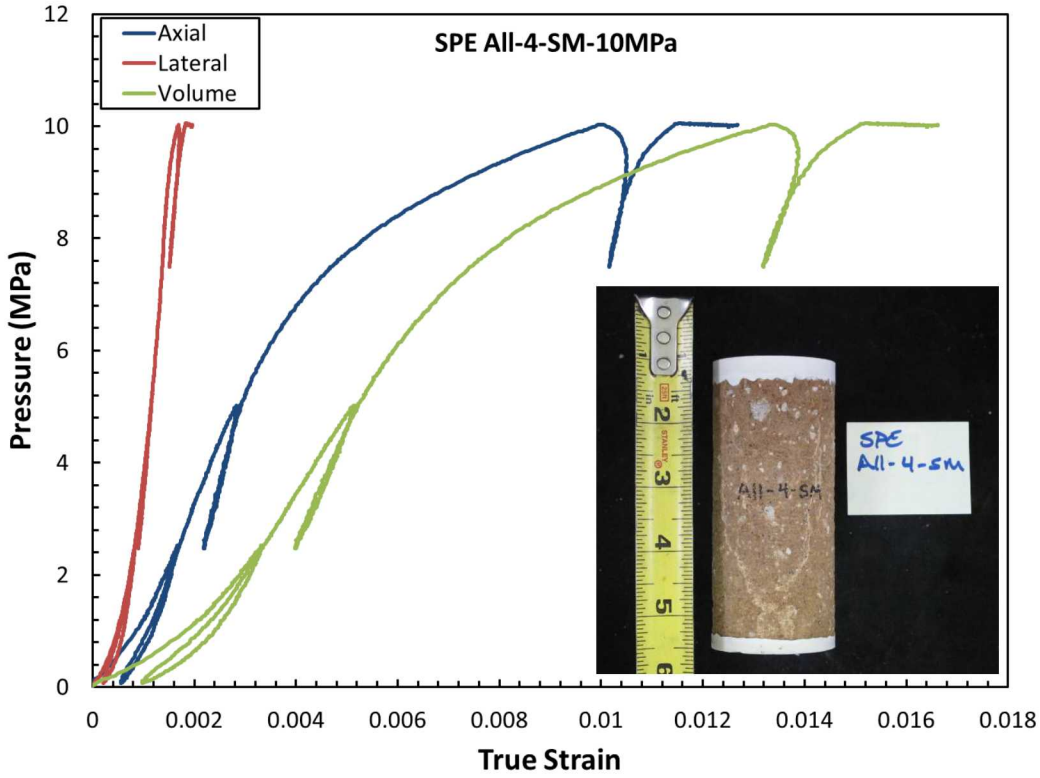

Figure A-7: Pressure versus strain plot for SPE All-4-SM-10MPa.

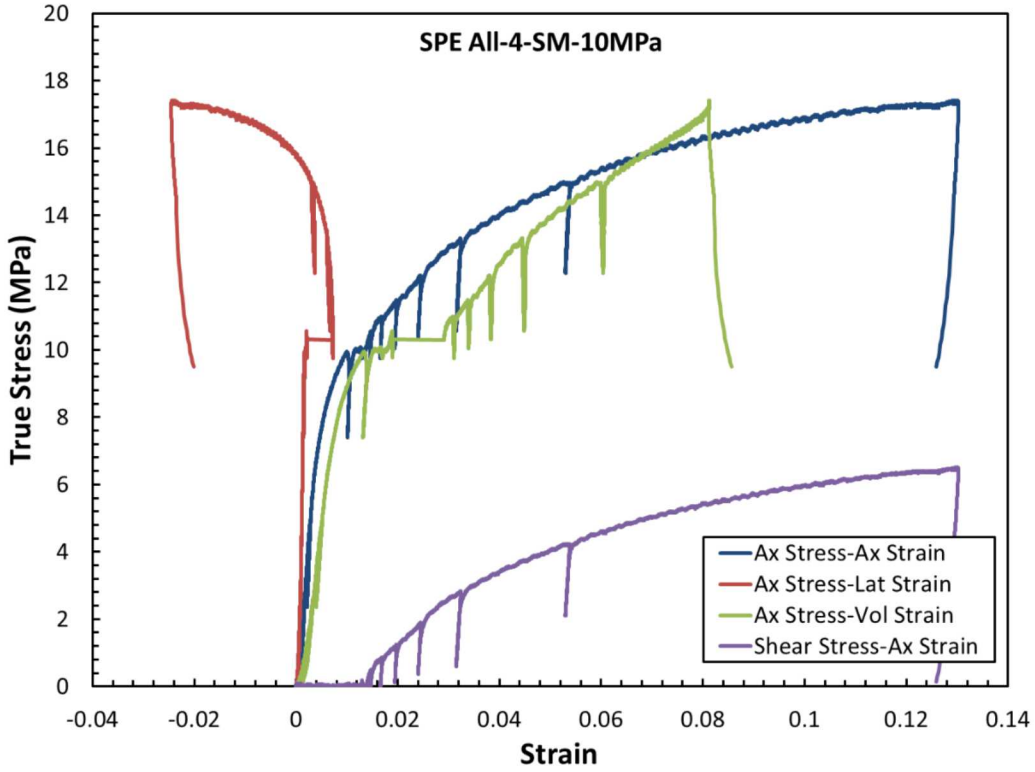

Figure A-8: Stress versus strain plot for SPE All-4-SM-10MPa.

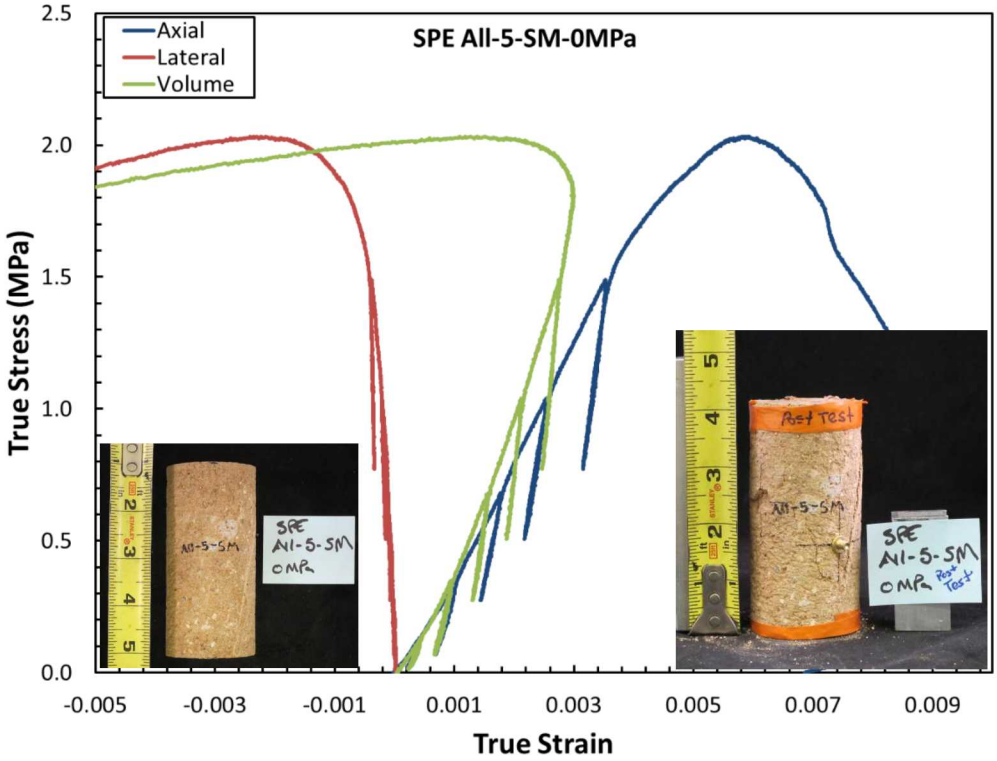

Figure A-9: Stress versus strain plot for SPE All-5-SM-0MPa.

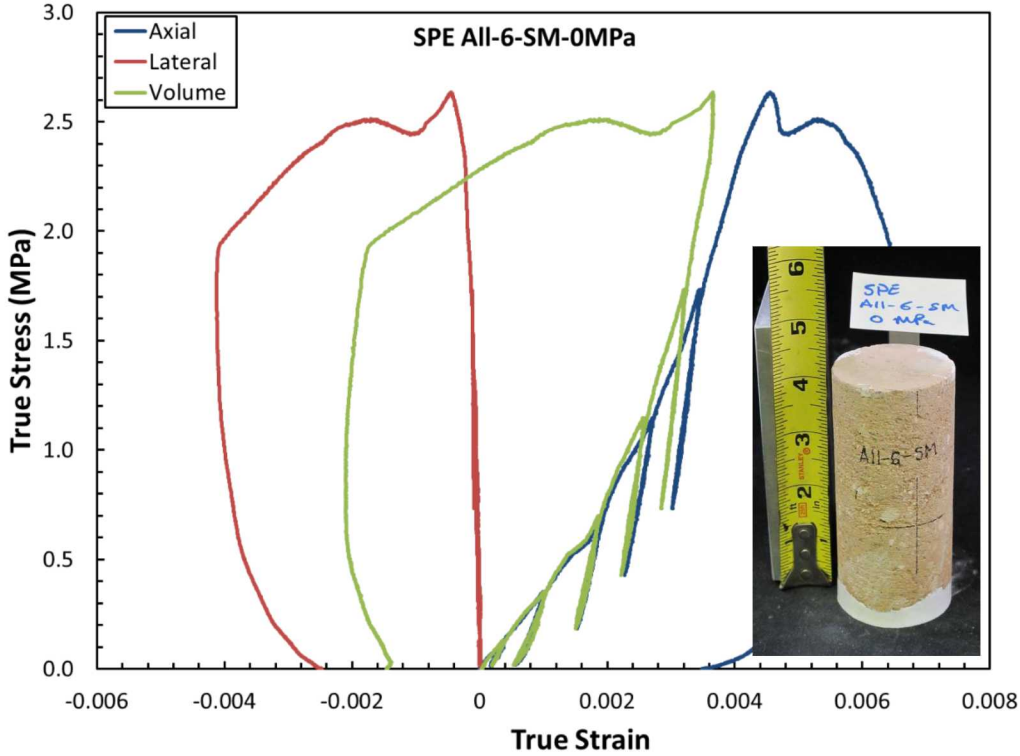

Figure A-10: Stress versus strain plot for SPE All-6-SM-0MPa.

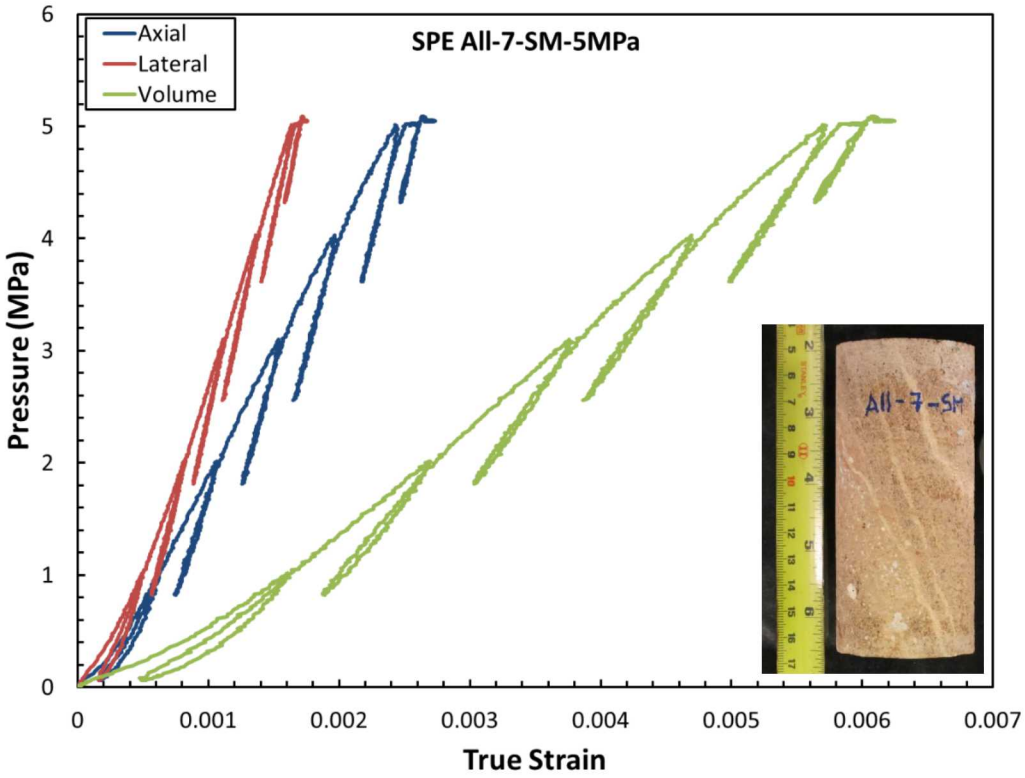

Figure A-11: Pressure versus strain plot for SPE All-7-SM-5MPa.

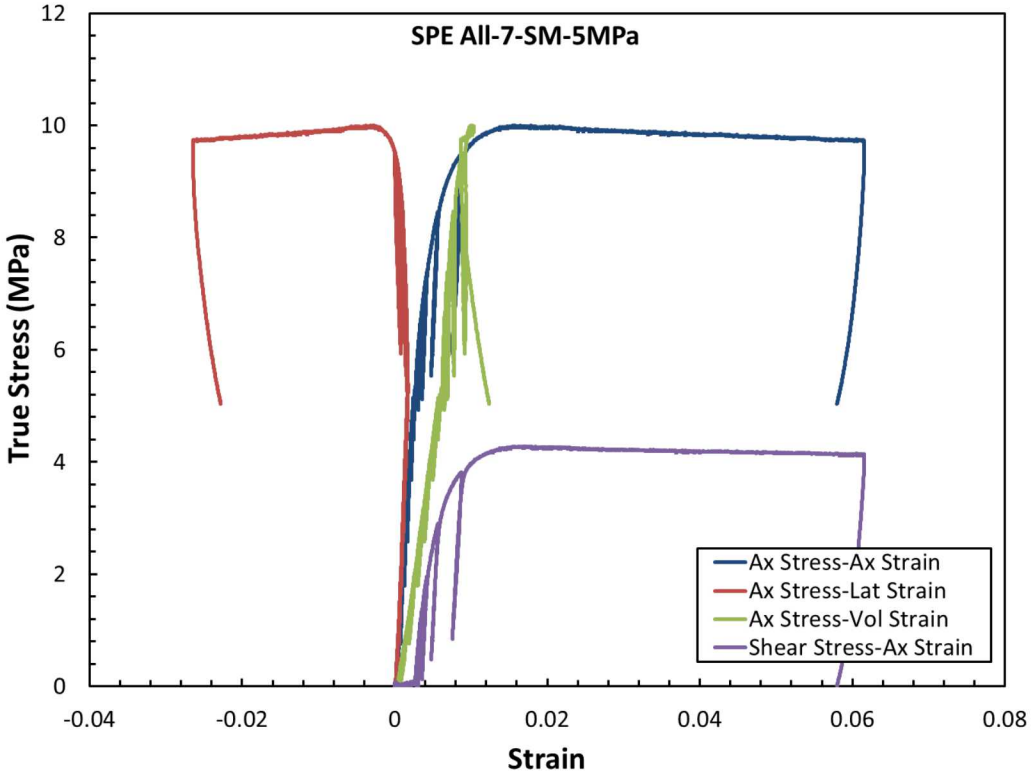

Figure A-12: Stress versus strain plot for SPE All-7-SM-5MPa.

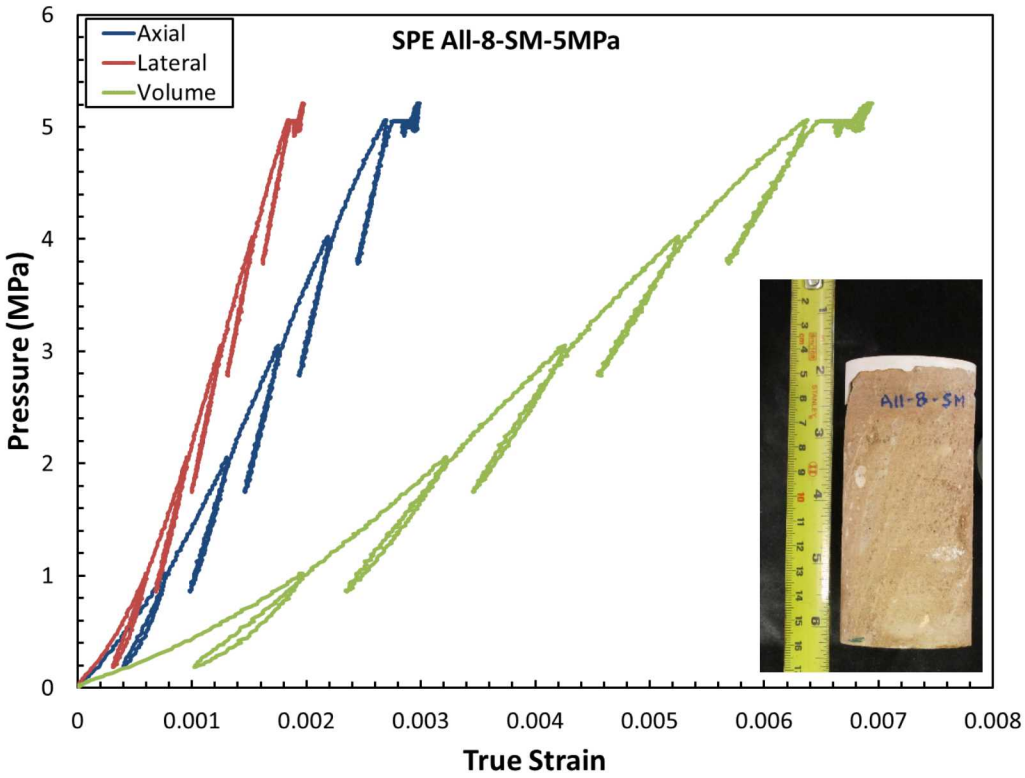

Figure A-13: Pressure versus strain plot for SPE All-8-SM-5MPa.

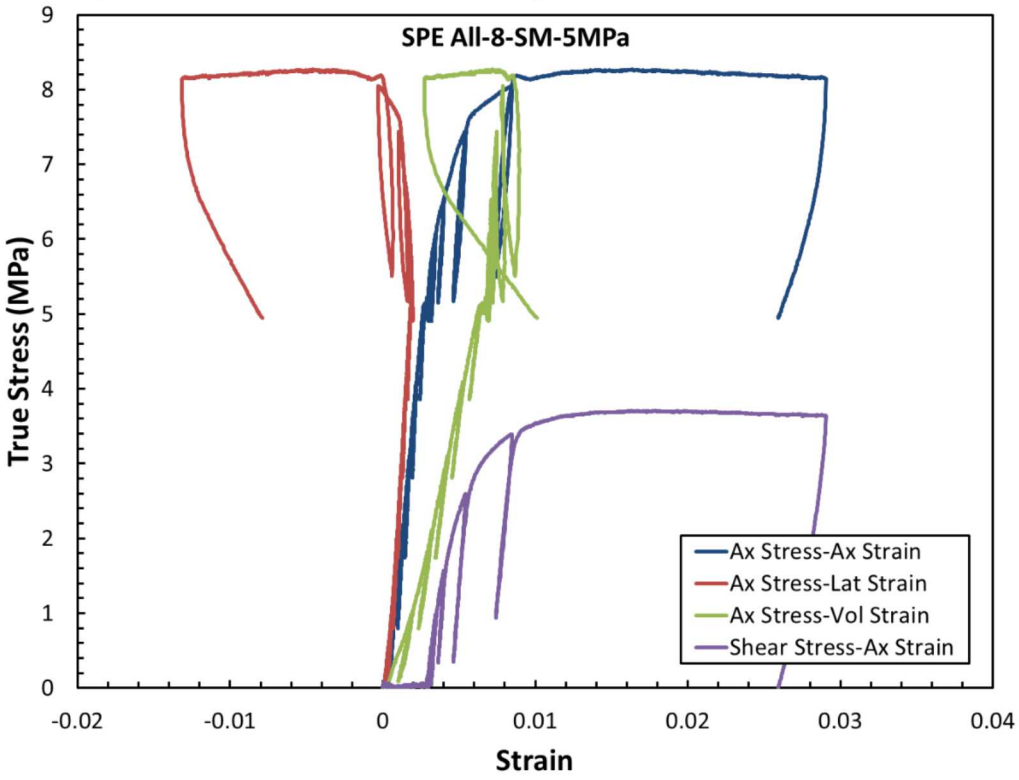

Figure A-14: Stress versus strain plot for SPE All-8-SM-5MPa.

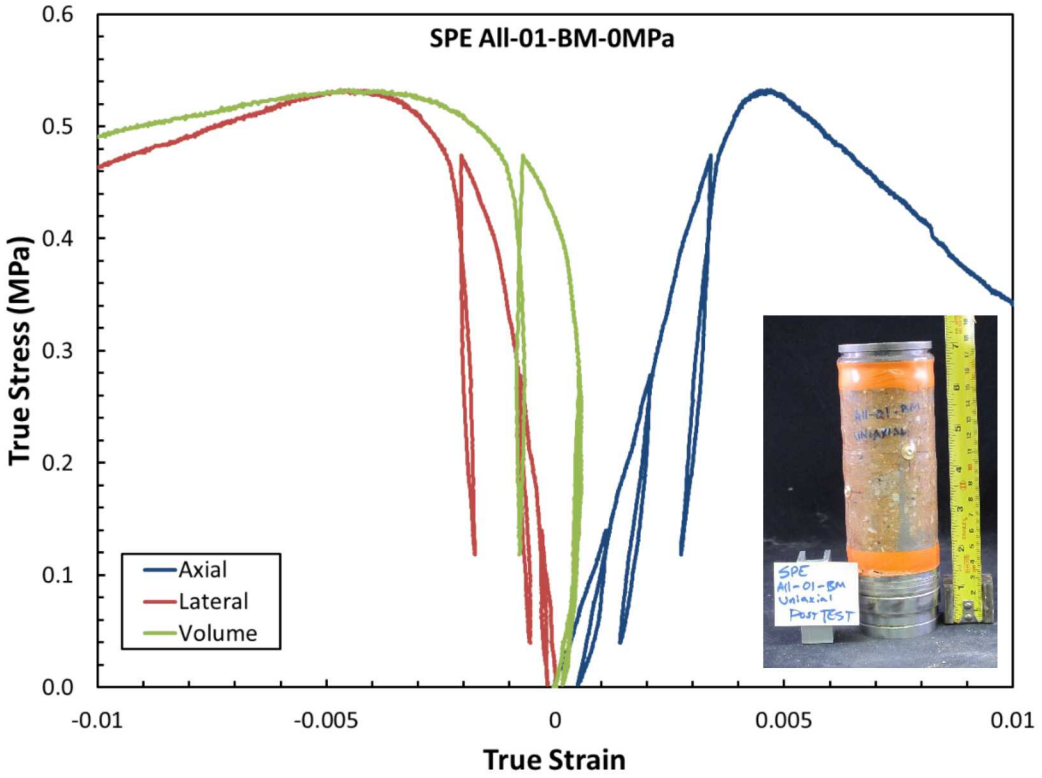

Figure A-15: Stress versus strain plot for SPE All-01-BM-0MPa.

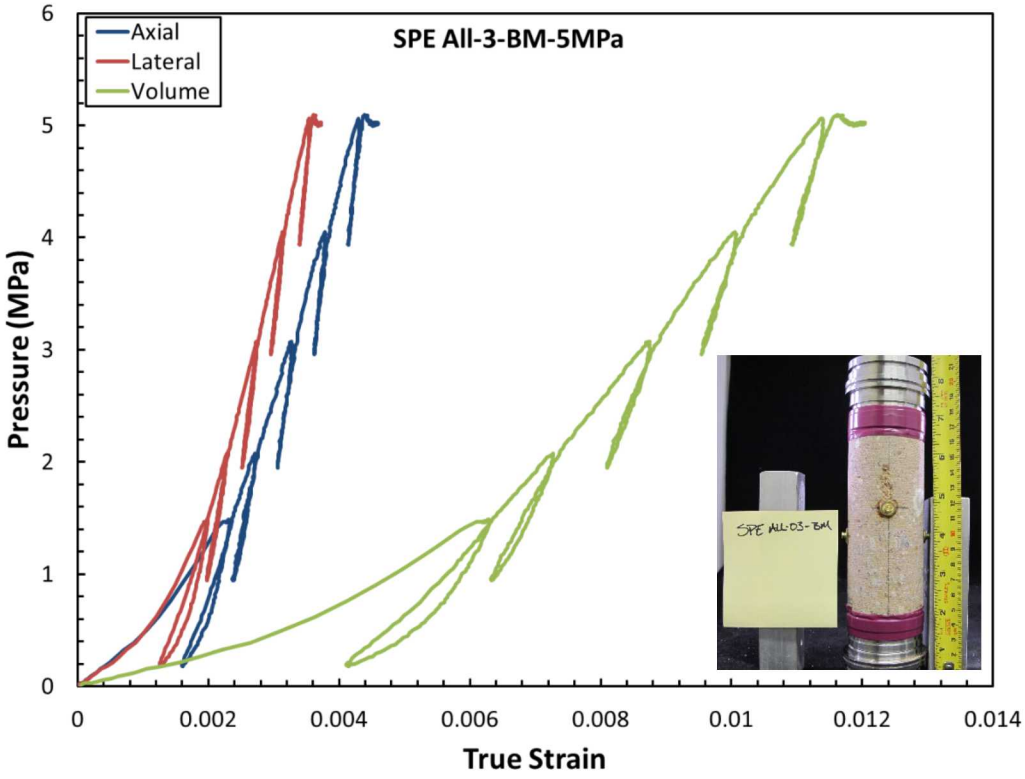

Figure A-16: Pressure versus strain plot for SPE All-03-BM-5MPa.

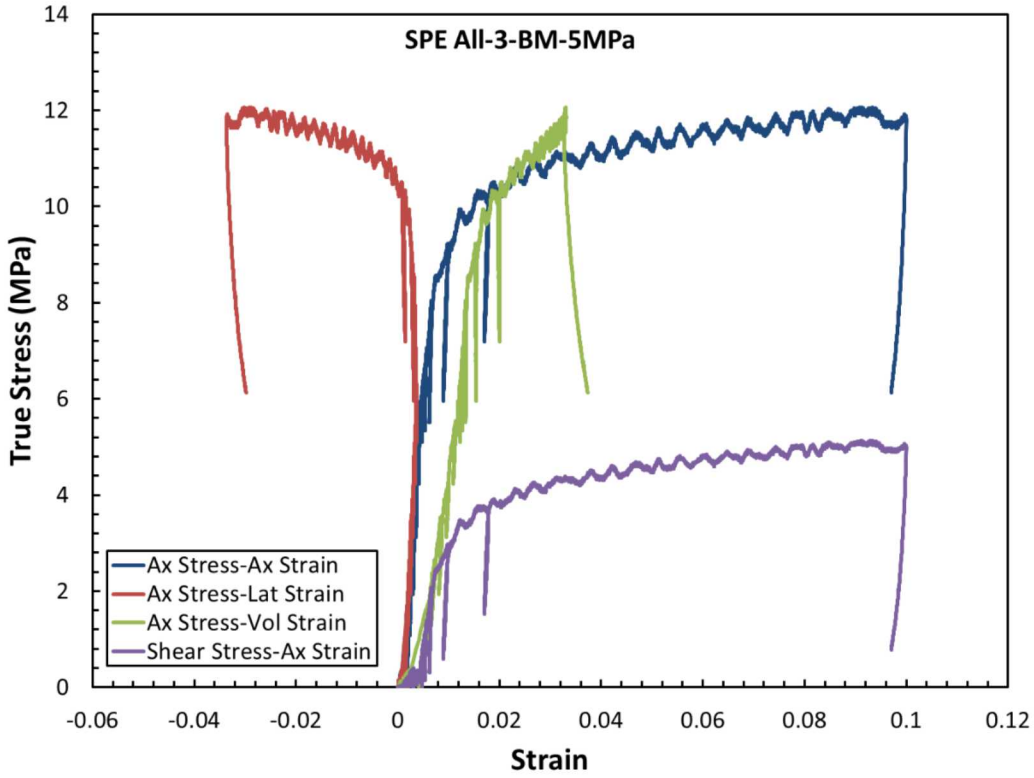

Figure A-17: Stress versus strain plot for SPE All-03-BM-5MPa.

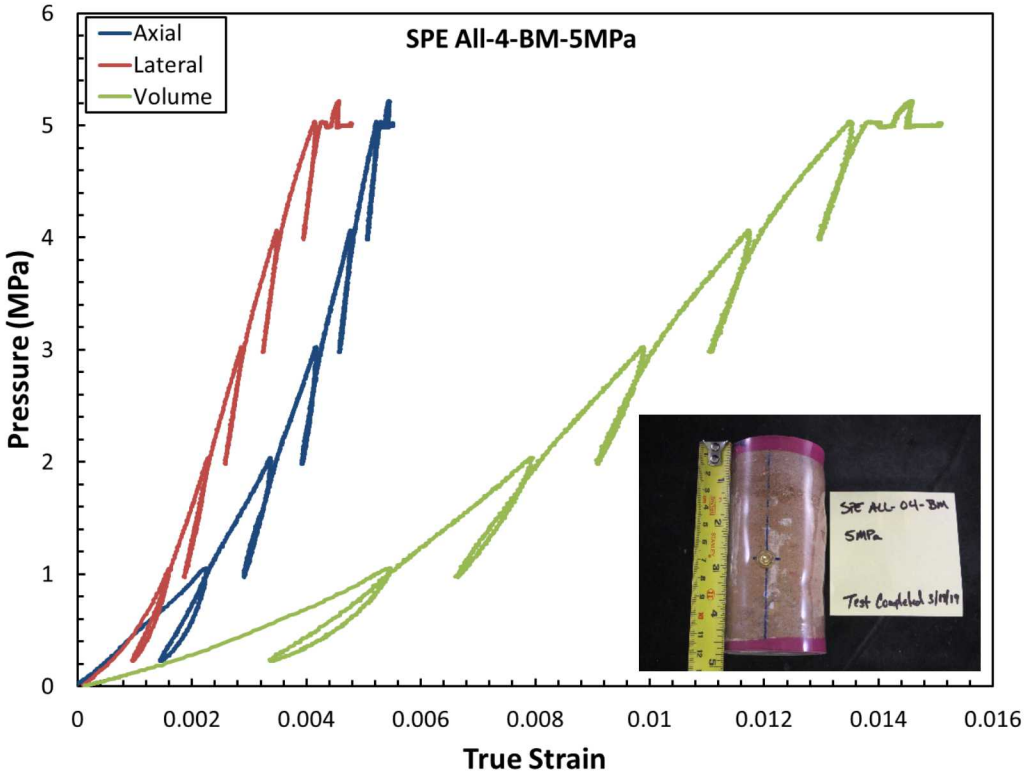

Figure A-18: Pressure versus strain plot for SPE All-04-BM-5MPa.

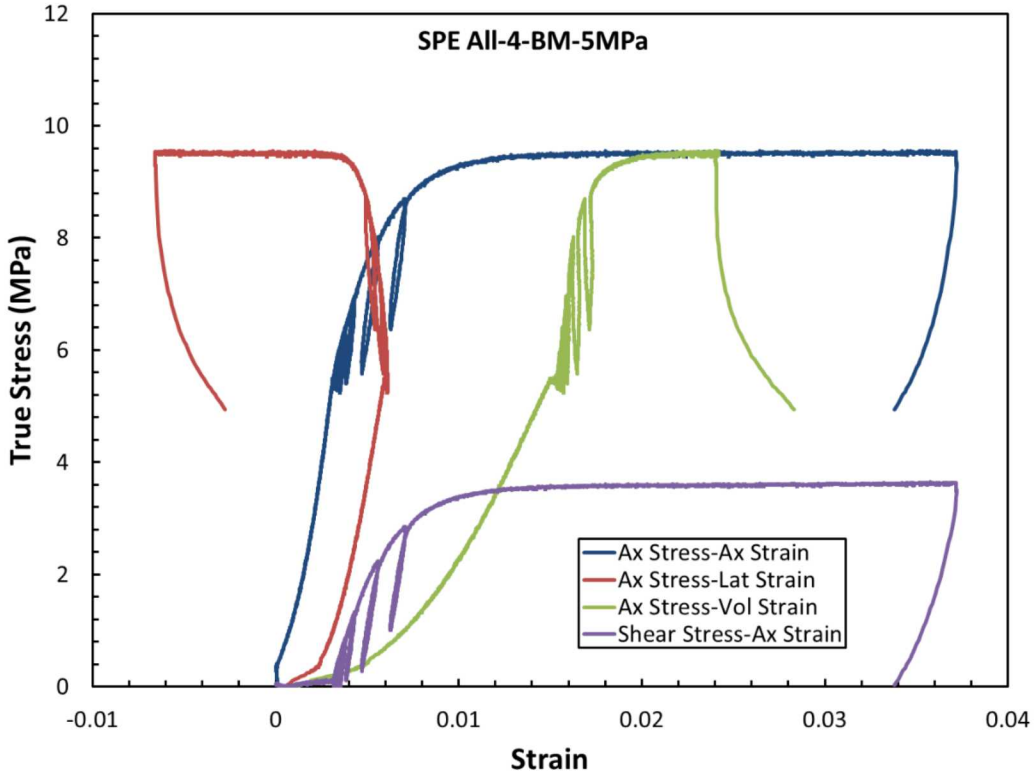

Figure A-19: Stress versus strain plot for SPE All-04-BM-5MPa.

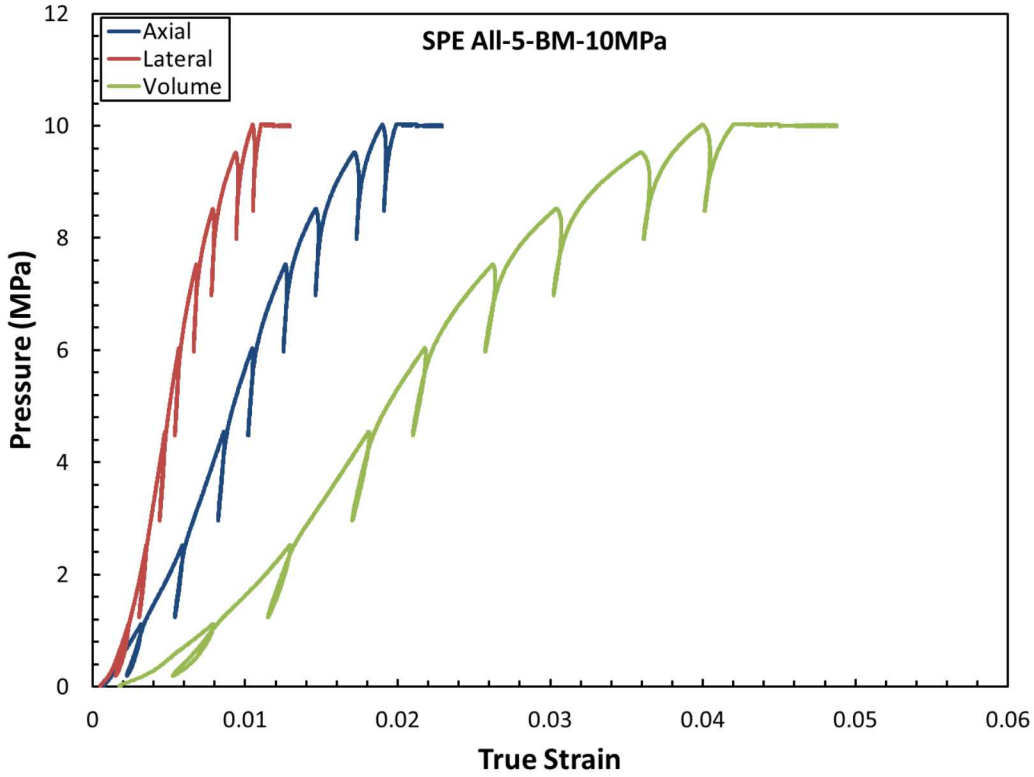

Figure A-20: Pressure versus strain plot for SPE All-05-BM-10MPa.

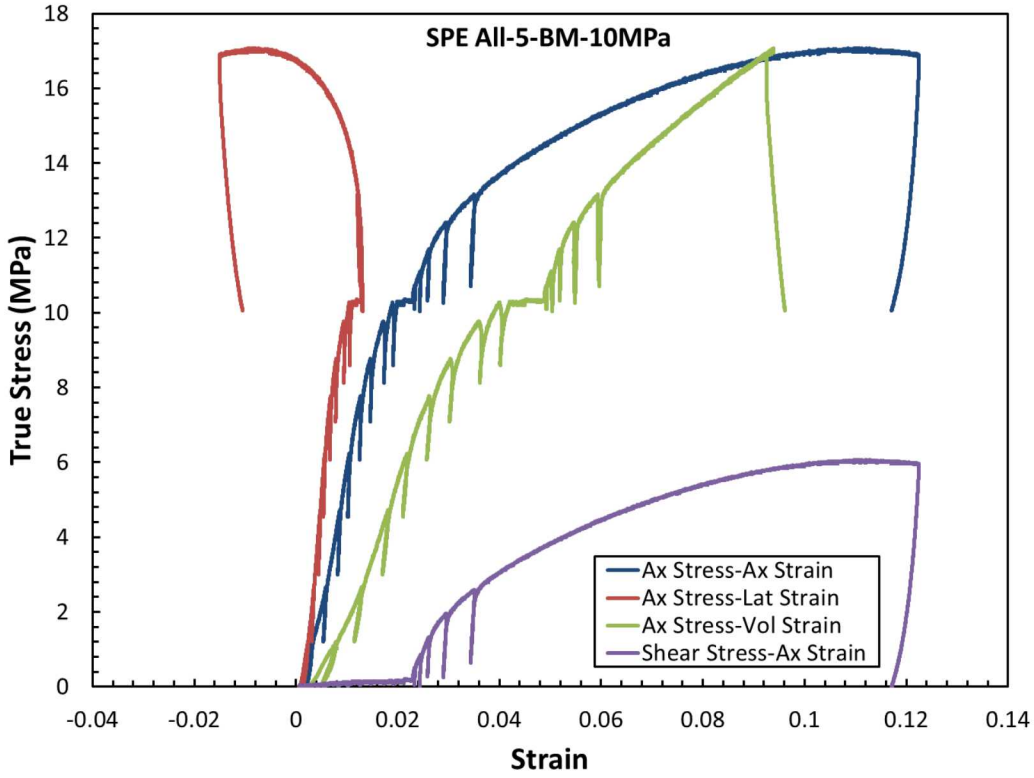

Figure A-21: Stress versus strain plot for SPE All-05-BM-10MPa.

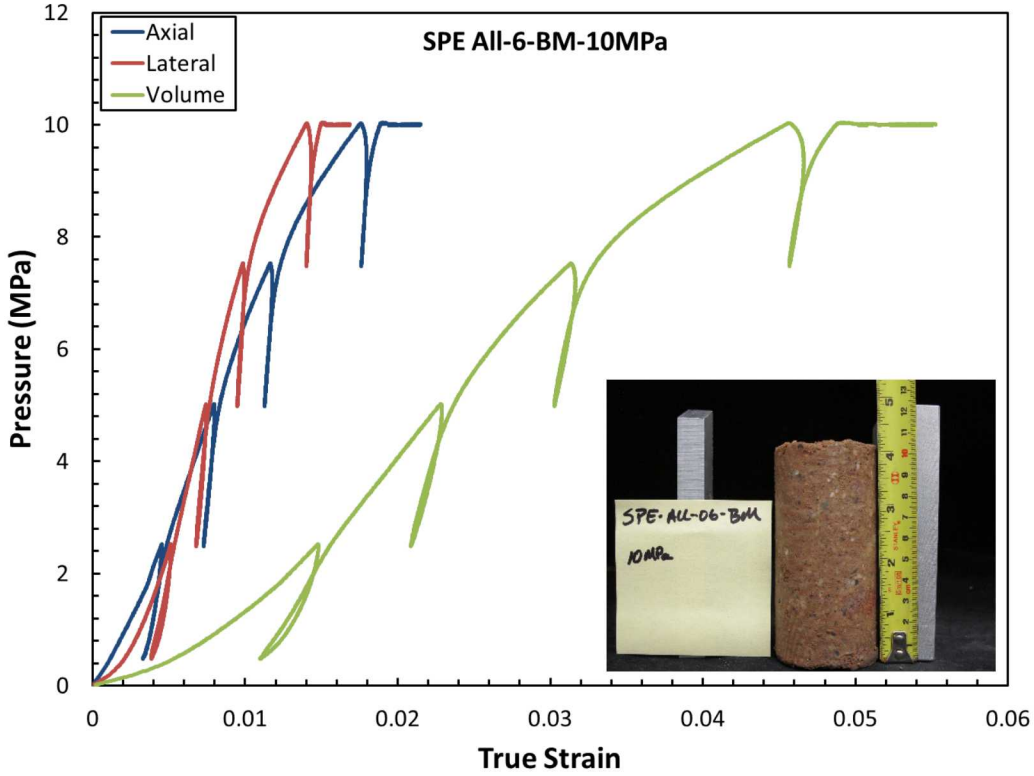

Figure A-22: Pressure versus strain plot for SPE All-06-BM-10MPa.

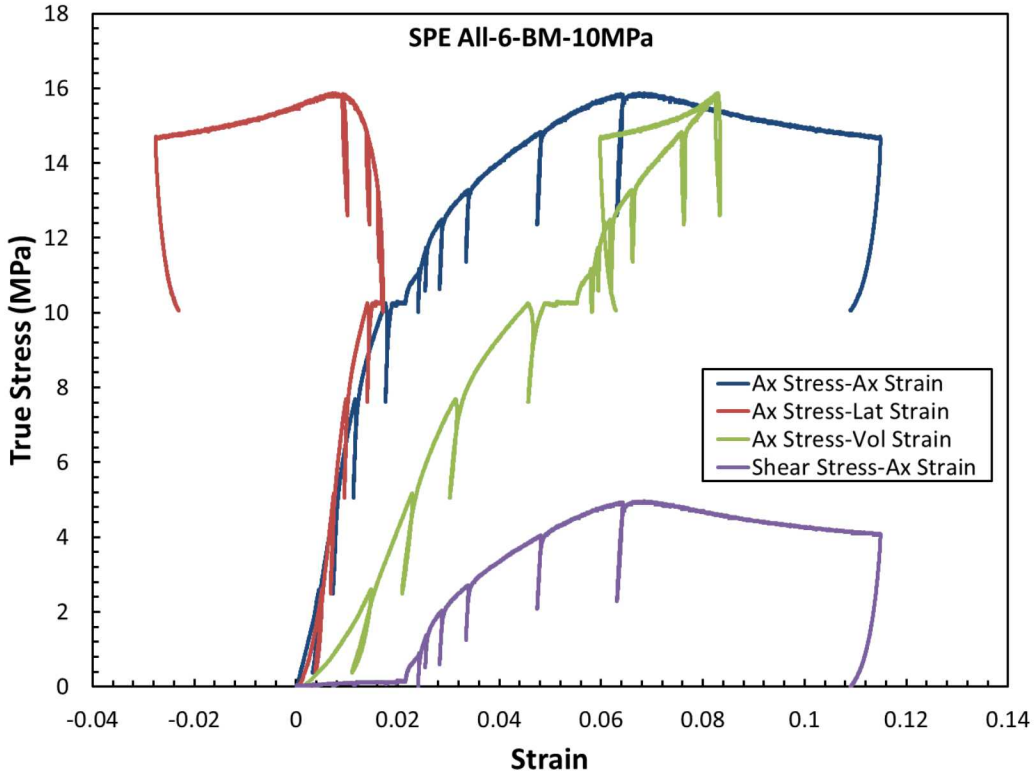

Figure A-23: Stress versus strain plot for SPE All-06-BM-10MPa.

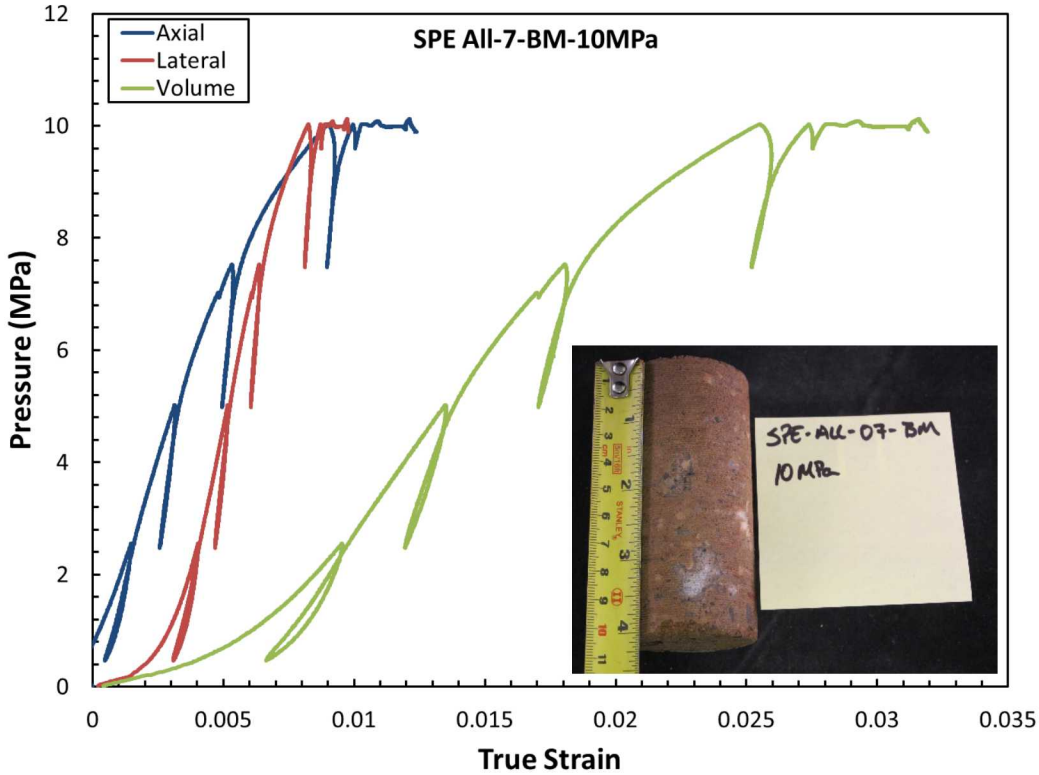

Figure A-24: Pressure versus strain plot for SPE All-07-BM-10MPa.

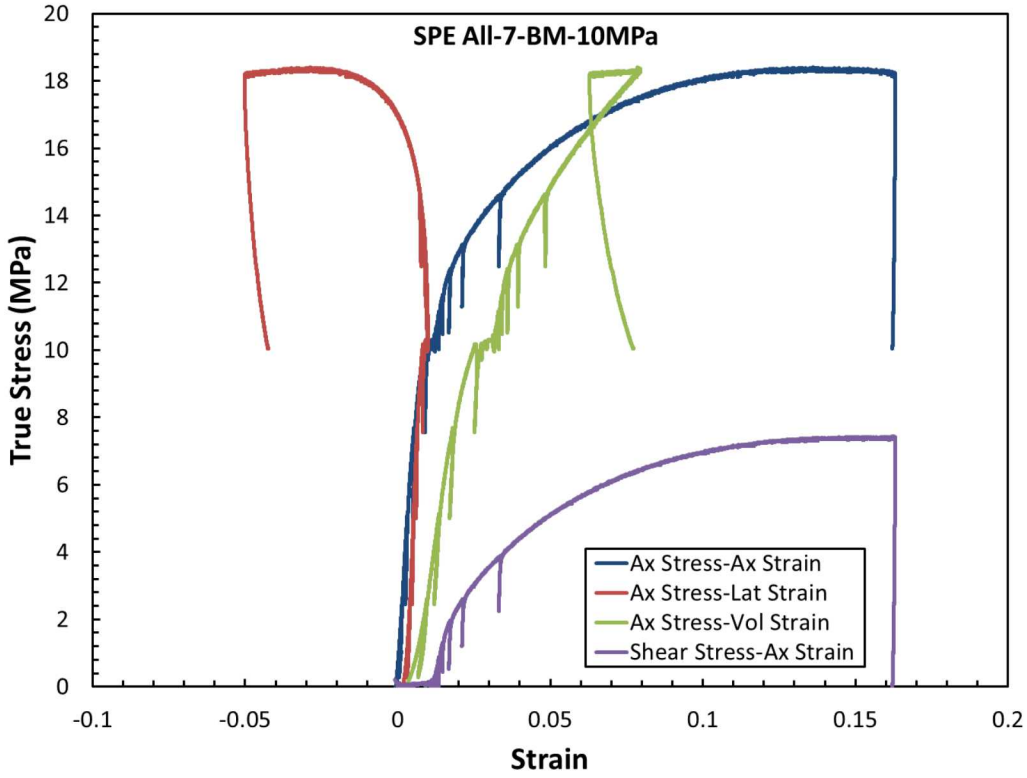

Figure A-25: Stress versus strain plot for SPE All-07-BM-10MPa.

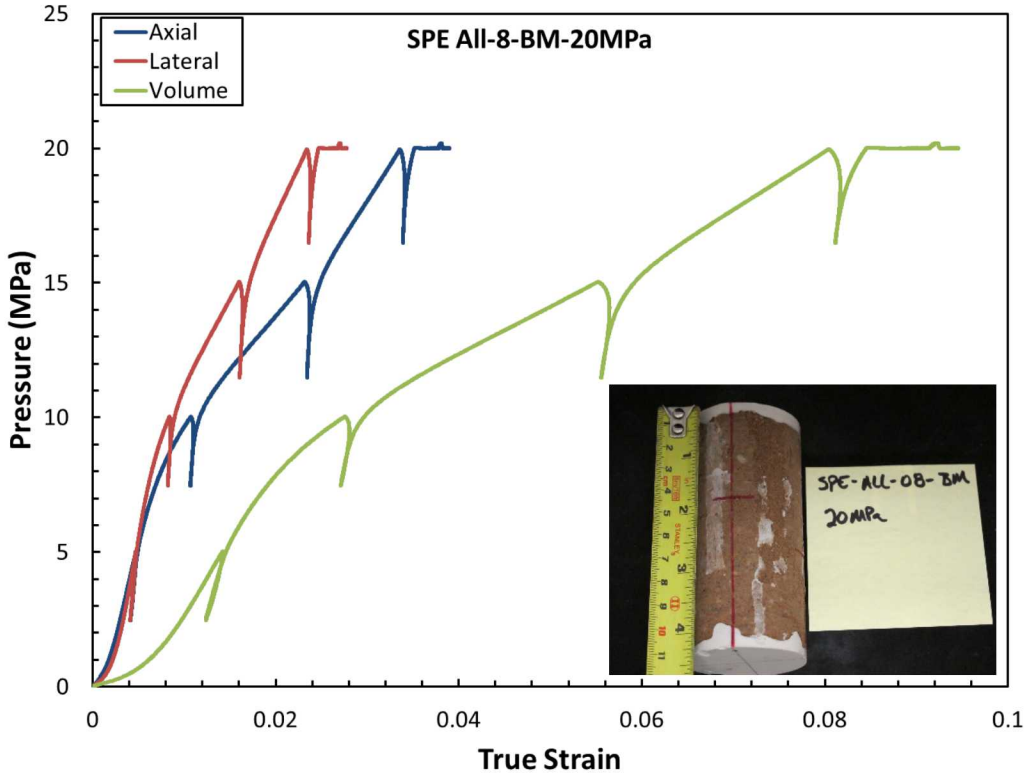

Figure A-26: Pressure versus strain plot for SPE All-08-BM-20MPa.

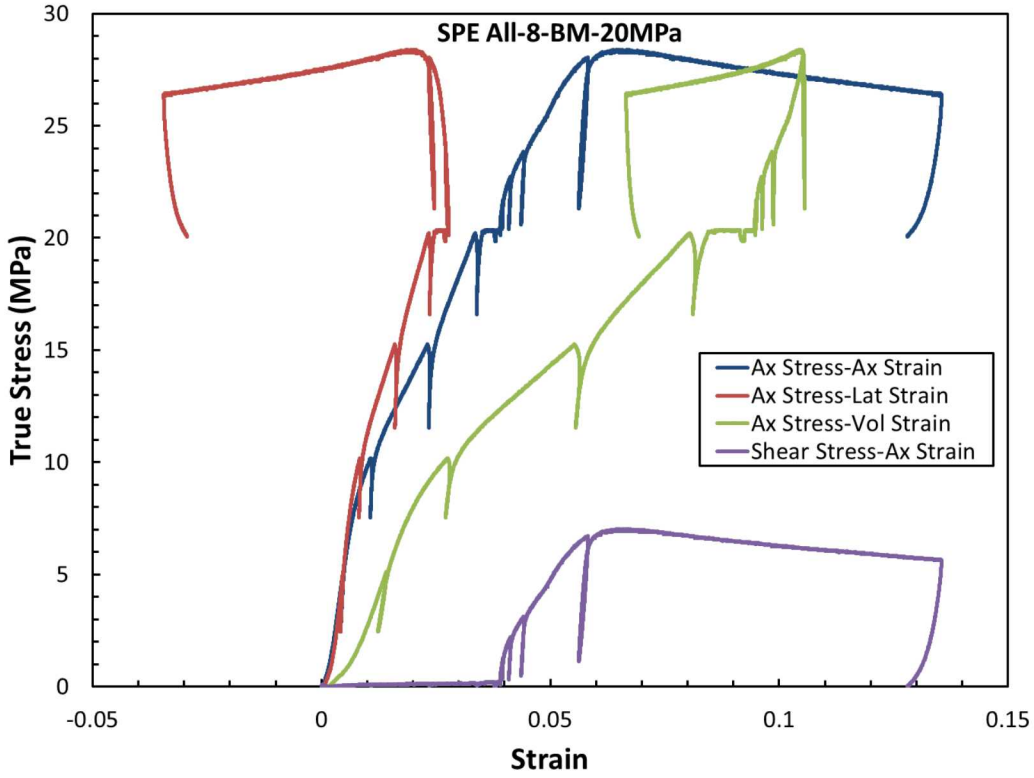

Figure A-27: Stress versus strain plot for SPE All-08-BM-20MPa.

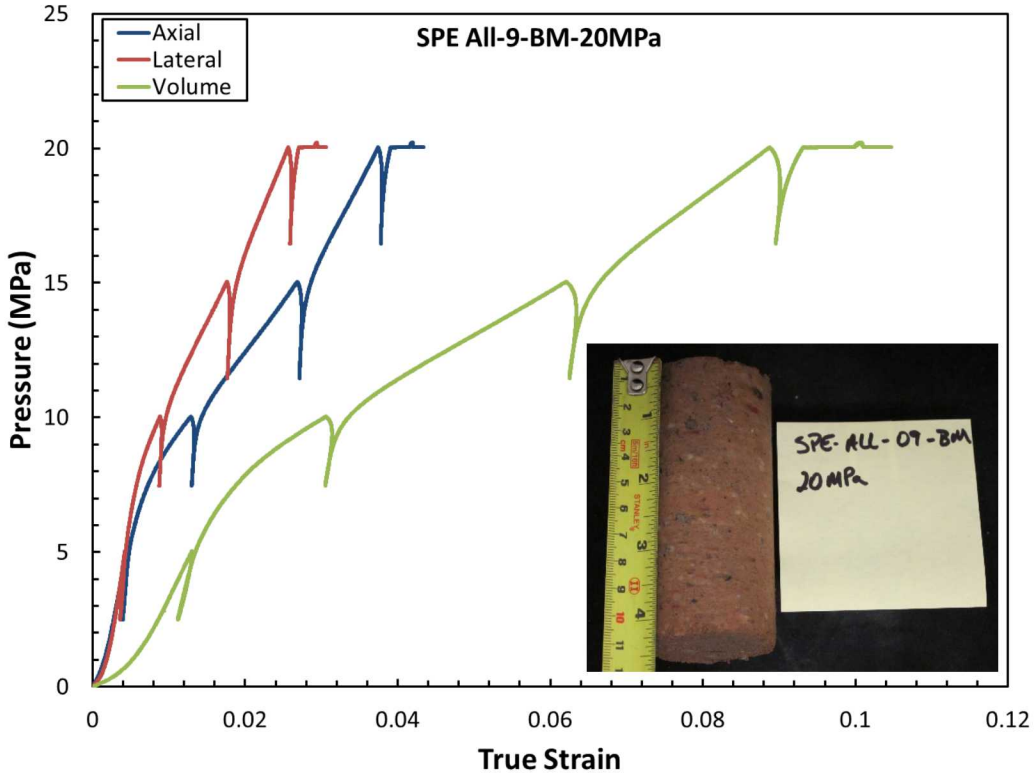

Figure A-28: Pressure versus strain plot for SPE All-09-BM-20MPa.

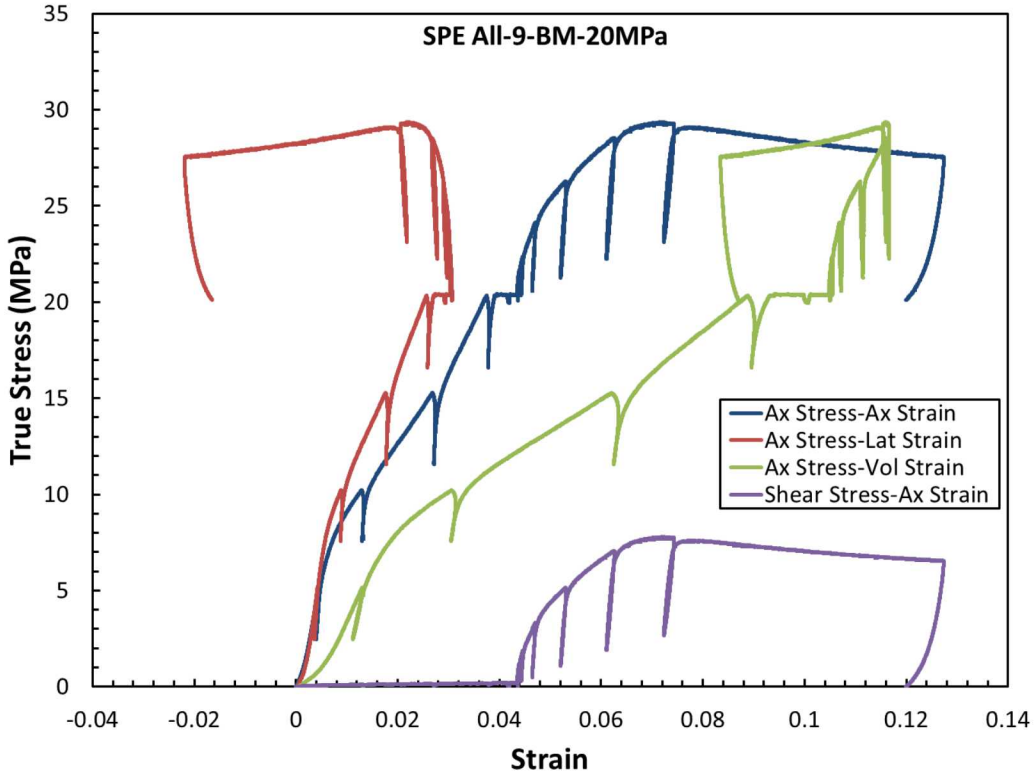

Figure A-29: Stress versus strain plot for SPE All-09-BM-20MPa.

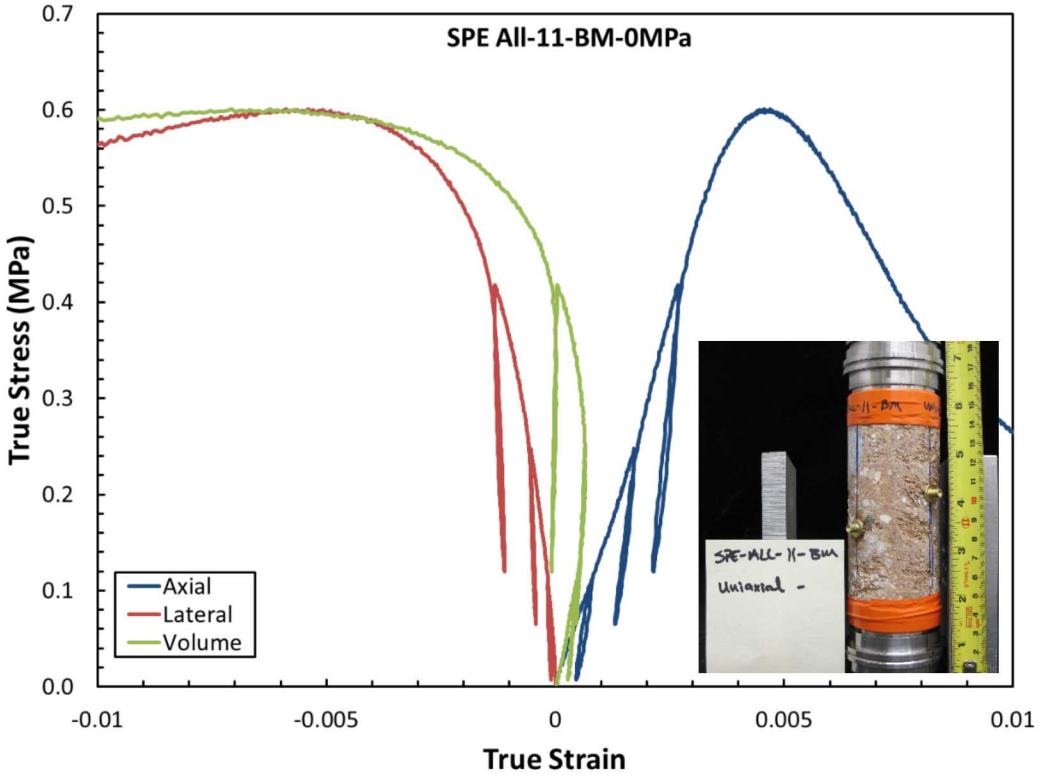

Figure A-30: Stress versus strain plot for SPE All-11-BM-0MPa.

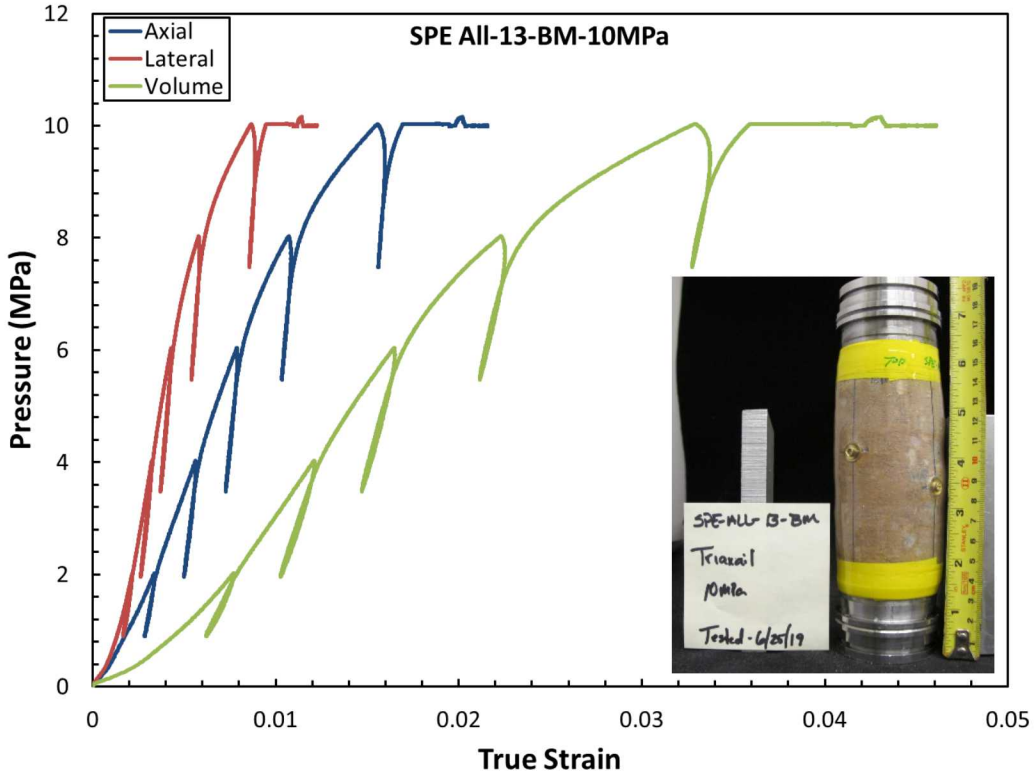

Figure A-31: Pressure versus strain plot for SPE All-13-BM-10MPa.

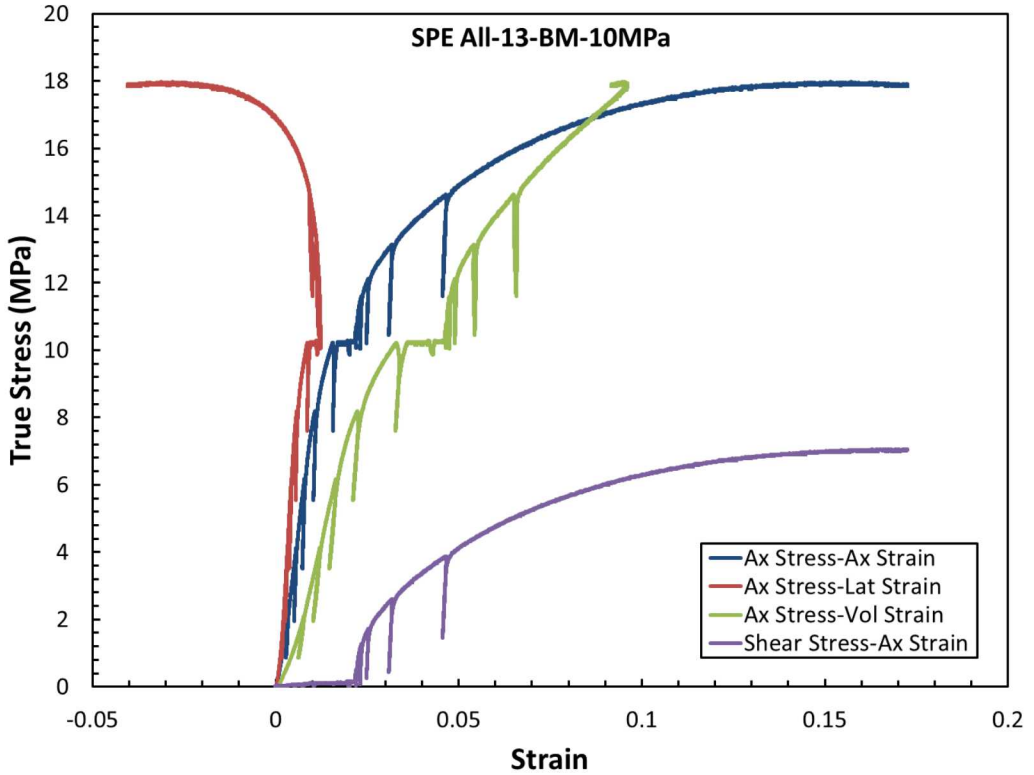

Figure A-32: Stress versus strain plot for SPE All-13-BM-10MPa.

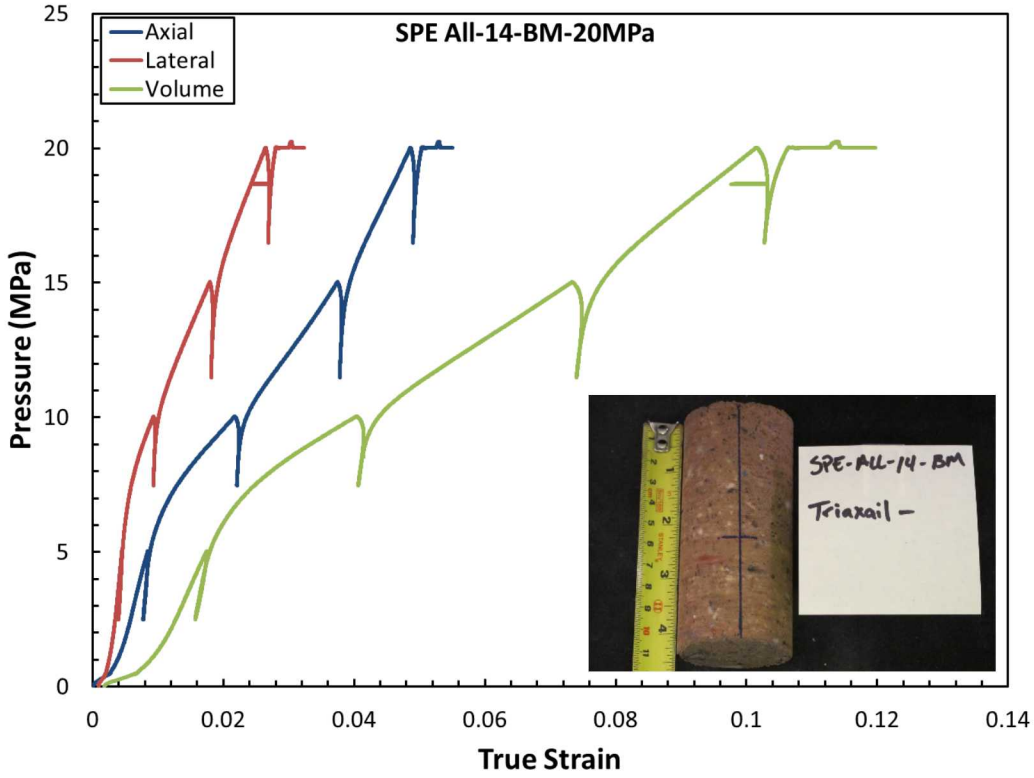

Figure A-33: Pressure versus strain plot for SPE All-14-BM-20MPa.

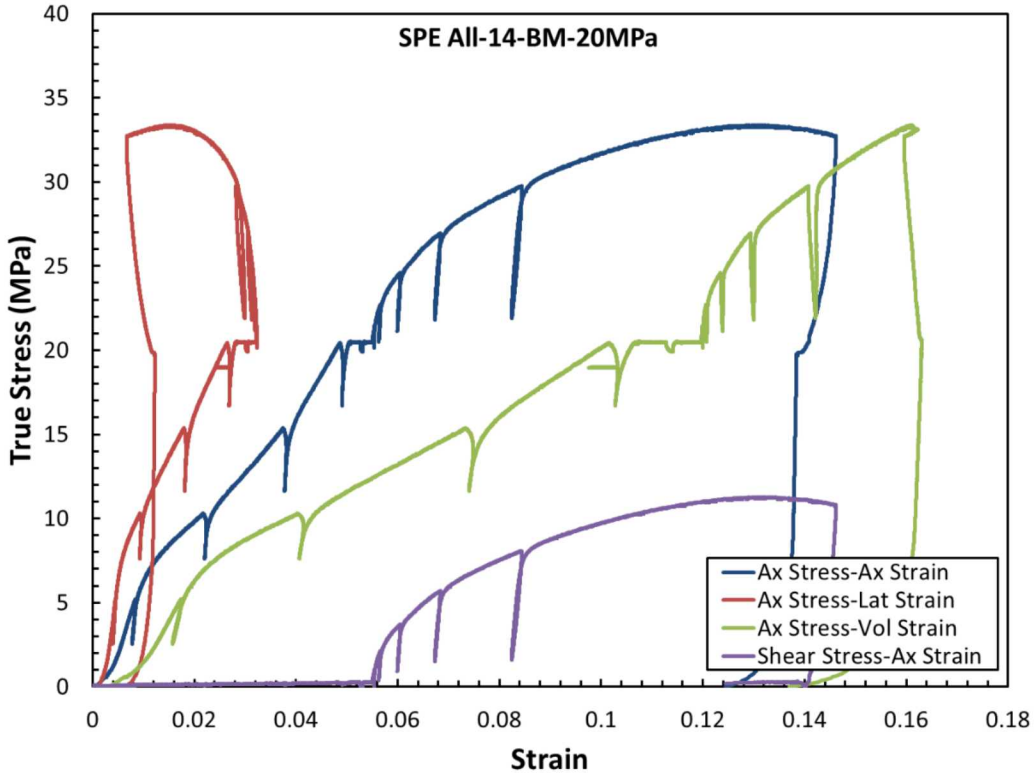

Figure A-34: Stress versus strain plot for SPE All-14-BM-20MPa.

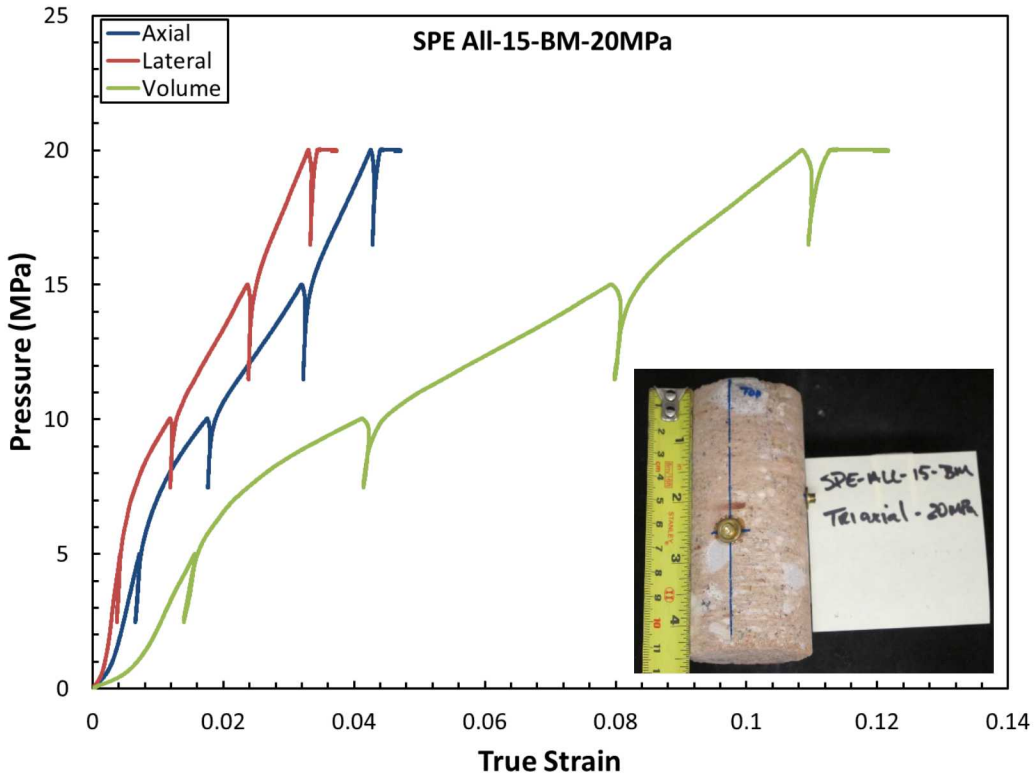

Figure A-35: Pressure versus strain plot for SPE All-15-BM-20MPa.

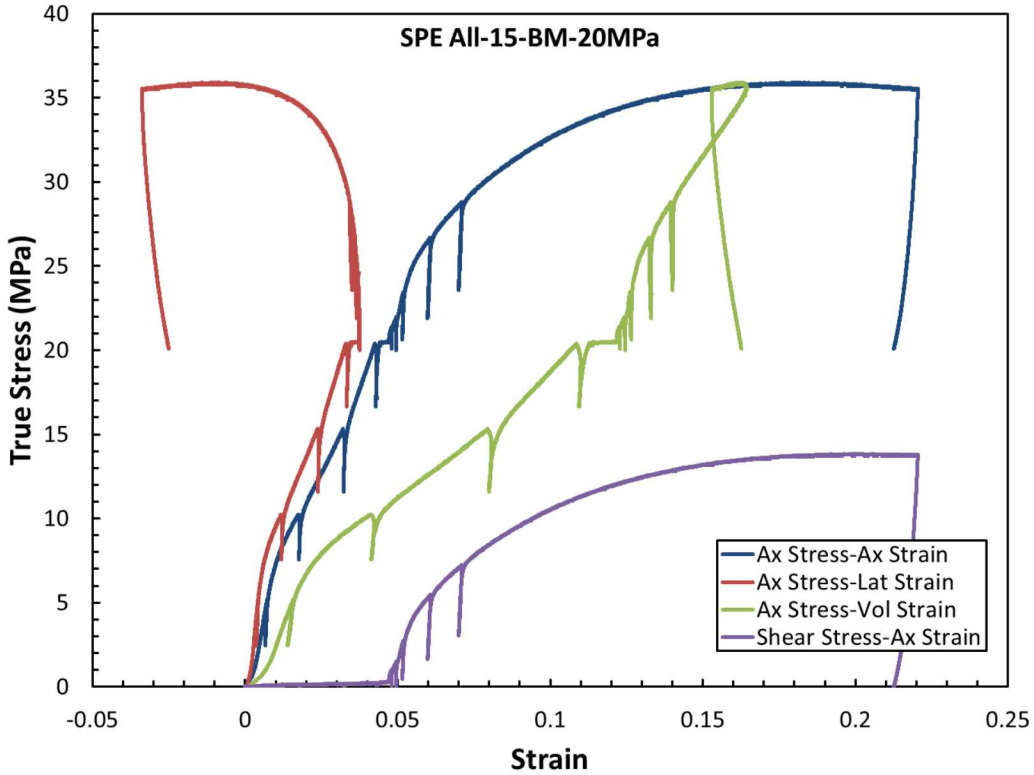

Figure A-36: Stress versus strain plot for SPE All-15-BM-20MPa.

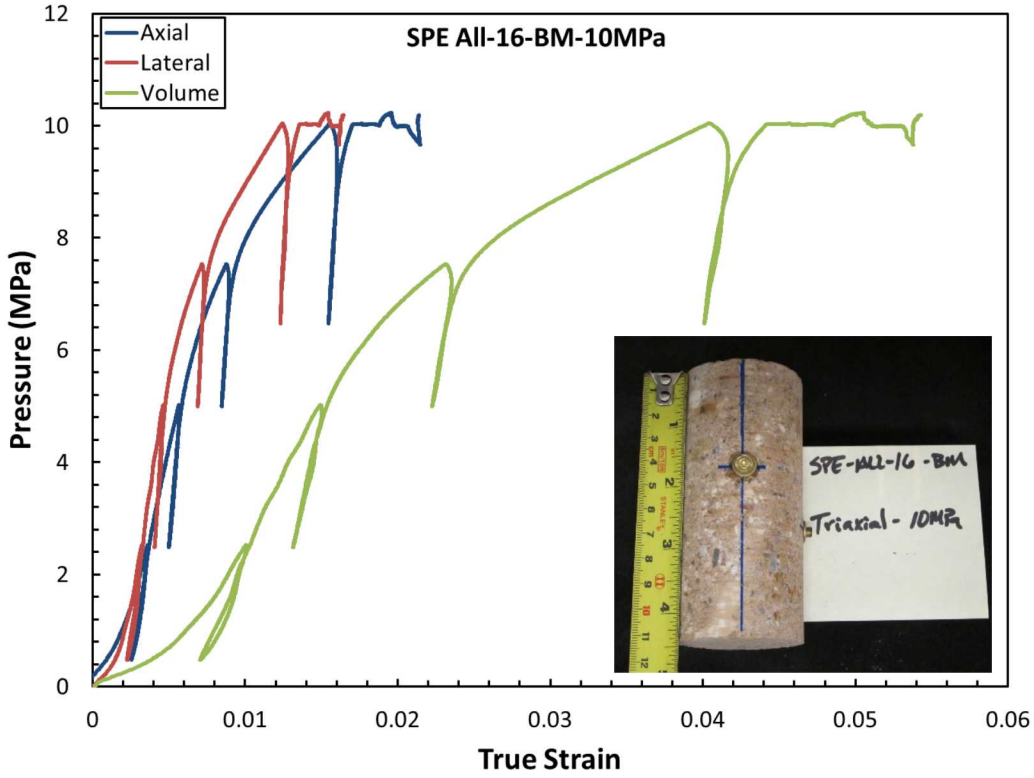

Figure A-37: Pressure versus strain plot for SPE All-16-BM-10MPa.

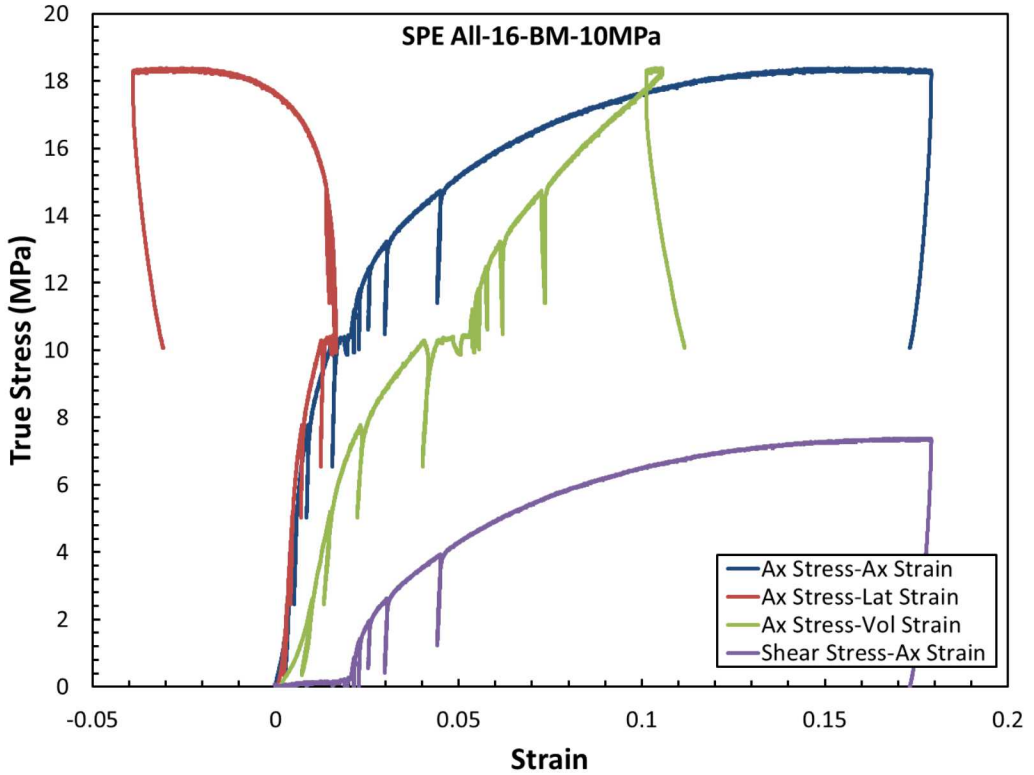

Figure A-38: Stress versus strain plot for SPE All-16-BM-10MPa.

APPENDIX B: PRESSURE VERSUS STRAIN PLOTS FOR HYDROSTATIC TESTS

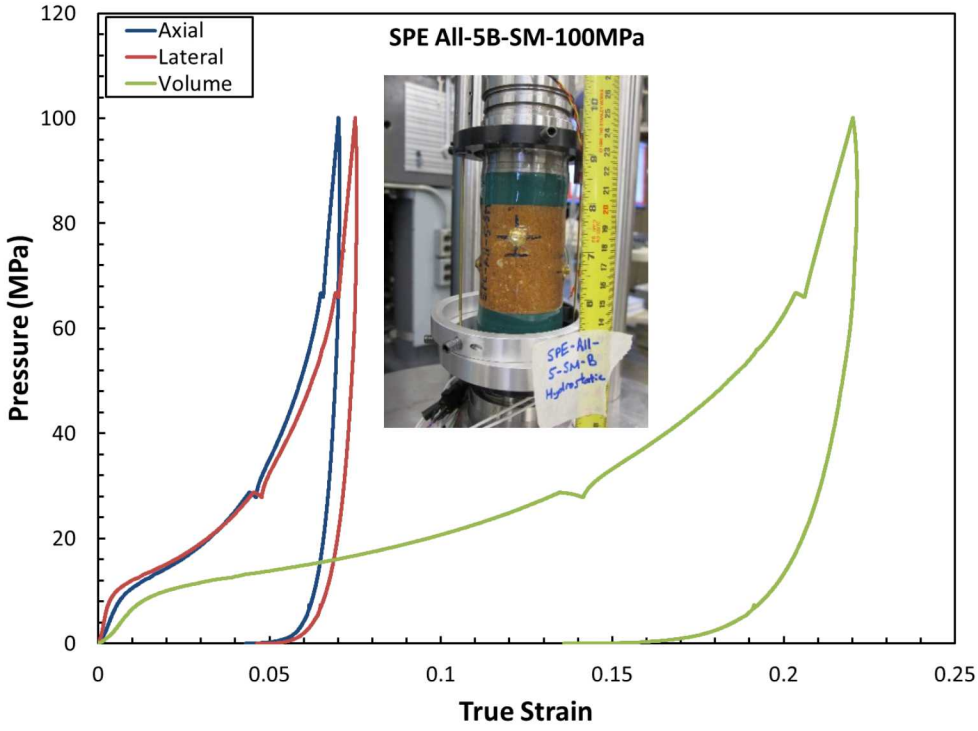

Figure B-1: Pressure versus strain plot for SPE All-5B-SM-100MPa.

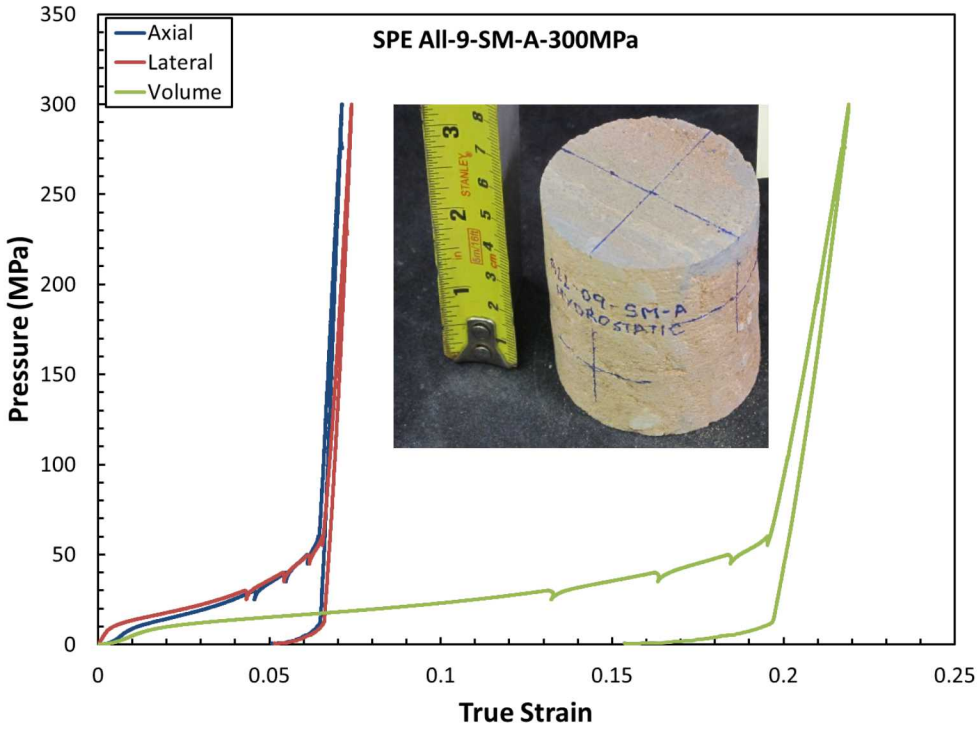

Figure B-2: Pressure versus strain plot for SPE All-9-SM-300MPa.

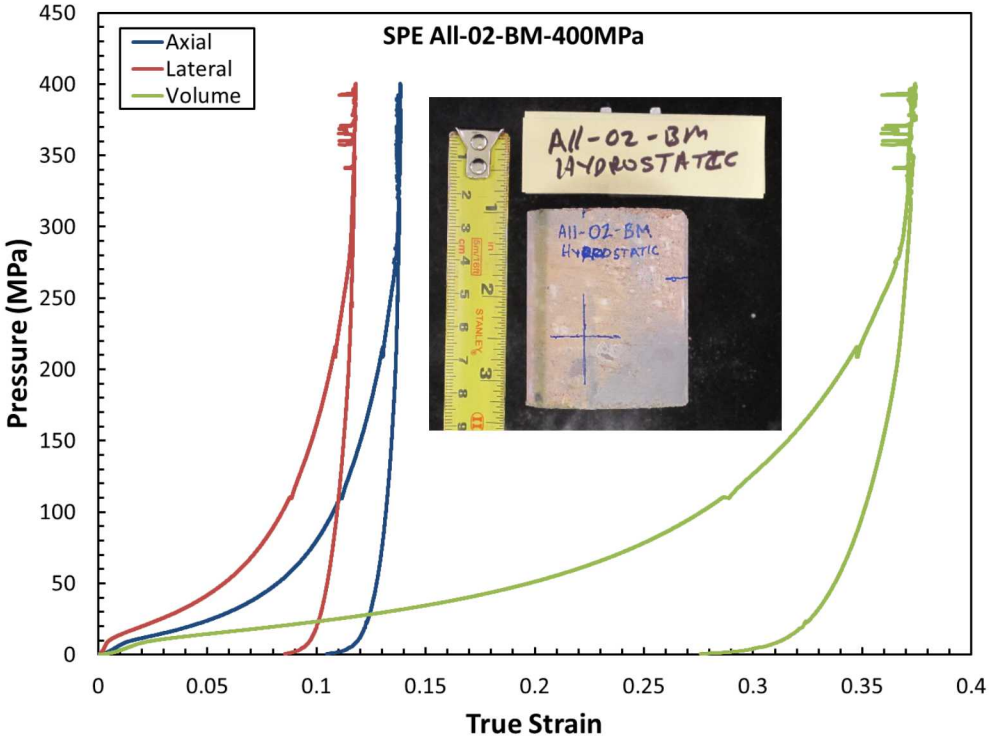

Figure B-3: Pressure versus strain plot for SPE All-02-BM-400MPa.

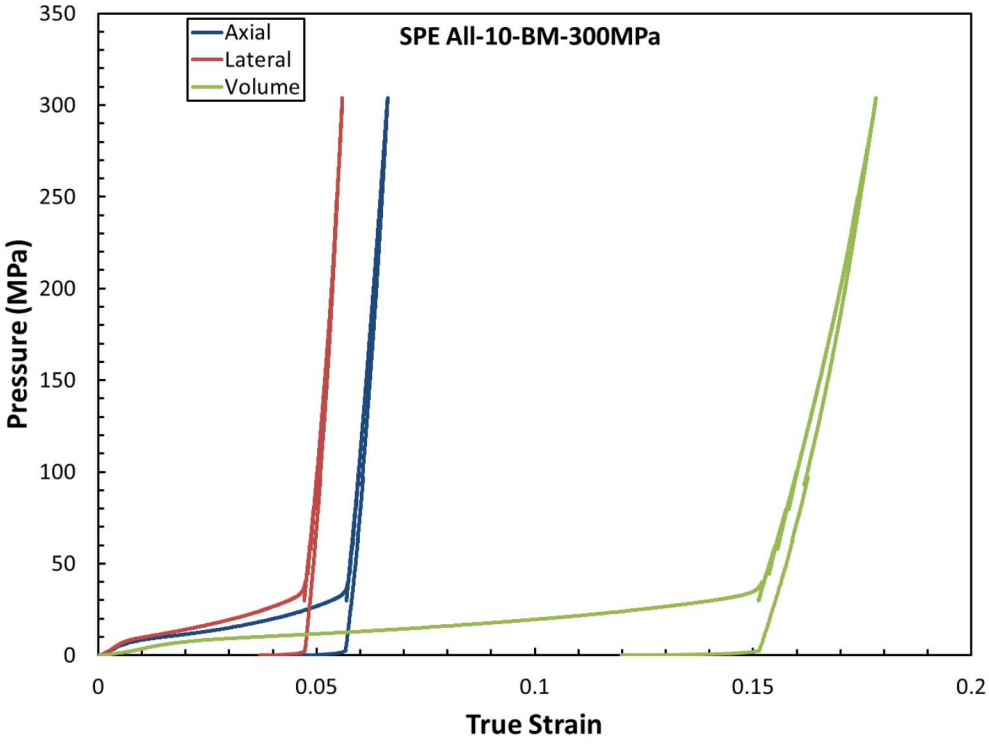

Figure B-4: Pressure versus strain plot for SPE All-10-BM-300MPa.

DISTRIBUTION

1	MS0735	Moo Lee	08864
1	MS0735	Kyle Jones	08861
1	MS0750	Robert Abbott	08861
1	MS1033	Scott Broome	08864
1	MS1033	Perry Barrow	08864
1	MS1033	Johnny Jaramillo	08864
1	MS0404	Steven Vigil	06752
1	MS0899	Technical Library	9536 (electronic copy)

Sandia National Laboratories